Developmental Cell

Article

DRMY1 promotes robust morphogenesis in *Arabidopsis* by sustaining the translation of cytokinin-signaling inhibitor proteins

Graphical abstract

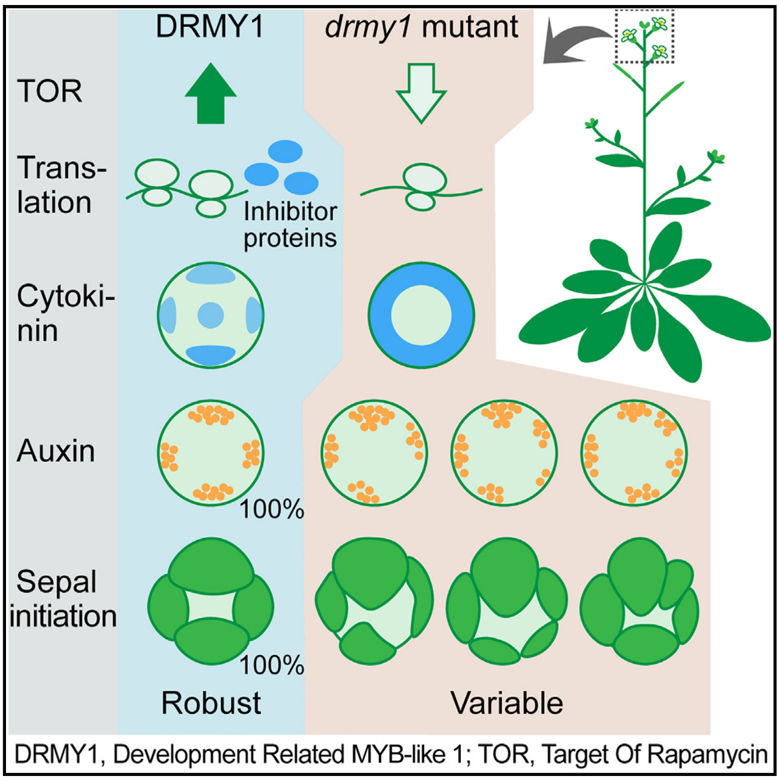

Authors

Shuyao Kong, Mingyuan Zhu,
M. Regina Scarpin, ..., Shu-Bing Qian,
Jacob O. Brunkard,
Adrienne H.K. Roeder

Correspondence

ahr75@cornell.edu

In brief

Developmental robustness is when organs develop to reproducible size, number, and arrangement, which Kong and Zhu et al. studied in sepals of the *Arabidopsis* plant. A transcription factor, DRMY1, maintains TOR signaling and translation, allowing strong synthesis of proteins key to robust hormone patterning and, thus, robust organogenesis.

Highlights

- DRMY1 promotes TOR signaling and protein synthesis in *Arabidopsis*
- High synthesis of ARR7 and AHP6 dampens cytokinin signaling in the floral meristem
- Low cytokinin signaling promotes robust auxin patterning and sepal initiation
- High cytokinin signaling in *drmy1* mutant may maintain protein synthesis homeostasis

Kong et al., 2024, Developmental Cell *59*, 1–20
December 2, 2024
https://doi.org/10.1016/j.devcel.2024.08.010

Please cite this article in press as: Kong et al., DRMY1 promotes robust morphogenesis in *Arabidopsis* by sustaining the translation of cytokinin-signaling inhibitor proteins, Developmental Cell (2024), https://doi.org/10.1016/j.devcel.2024.08.010

Developmental Cell

CellPress

Article

DRMY1 promotes robust morphogenesis in *Arabidopsis* by sustaining the translation of cytokinin-signaling inhibitor proteins

Shuyao Kong,[1,2,14] Mingyuan Zhu,[1,2,13,14] M. Regina Scarpin,[3] David Pan,[1,2] Longfei Jia,[4] Ryan E. Martinez,[3] Simon Alamos,[5,6,7] Batthula Vijaya Lakshmi Vadde,[1,2] Hernan G. Garcia,[8,9,10,11,12] Shu-Bing Qian,[4] Jacob O. Brunkard,[3] and Adrienne H.K. Roeder[1,2,15,*]

[1]Weill Institute for Cell and Molecular Biology, Cornell University, Ithaca, NY 14853, USA
[2]Section of Plant Biology, School of Integrative Plant Science, Cornell University, Ithaca, NY 14853, USA
[3]Laboratory of Genetics, University of Wisconsin, Madison, WI 53706, USA
[4]Division of Nutritional Sciences, Cornell University, Ithaca, NY 14853, USA
[5]Environmental Genomics and Systems Biology Division, Lawrence Berkeley National Laboratory, Berkeley, CA 94720, USA
[6]Feedstocks Division, Joint BioEnergy Institute, Emeryville, CA 94608, USA
[7]Department of Plant and Microbial Biology, University of California at Berkeley, Berkeley, CA 94720, USA
[8]Biophysics Graduate Group, University of California at Berkeley, Berkeley, CA 94720, USA
[9]Department of Physics, University of California at Berkeley, Berkeley, CA 94720, USA
[10]Institute for Quantitative Biosciences-QB3, University of California at Berkeley, Berkeley, CA 94720, USA
[11]Department of Molecular and Cell Biology, University of California at Berkeley, Berkeley, CA 94720, USA
[12]Chan Zuckerberg Biohub, San Francisco, San Francisco, CA 94158, USA
[13]Present address: Department of Biology, Duke University, Durham, NC 27708, USA
[14]These authors contributed equally
[15]Lead contact
*Correspondence: ahr75@cornell.edu
https://doi.org/10.1016/j.devcel.2024.08.010

SUMMARY

Robustness is the invariant development of phenotype despite environmental changes and genetic perturbations. In the *Arabidopsis* flower bud, four sepals robustly initiate and grow to a constant size to enclose and protect the inner floral organs. We previously characterized the mutant *development-related myb-like 1* (*drmy1*), where 3–5 sepals initiate variably and grow to different sizes, compromising their protective function. The molecular mechanism underlying this loss of robustness was unclear. Here, we show that *drmy1* has reduced TARGET OF RAPAMYCIN (TOR) activity, ribosomal content, and translation. Translation reduction decreases the protein level of *ARABIDOPSIS* RESPONSE REGULATOR7 (ARR7) and *ARABIDOPSIS* HISTIDINE PHOSPHOTRANSFER PROTEIN 6 (AHP6), two cytokinin-signaling inhibitors that are normally rapidly produced before sepal initiation. The resultant upregulation of cytokinin signaling disrupts robust auxin patterning and sepal initiation. Our work shows that the homeostasis of translation, a ubiquitous cellular process, is crucial for the robust spatiotemporal patterning of organogenesis.

INTRODUCTION

Robustness, or canalization, is the invariant, reproducible development of phenotype, unchanged by environmental fluctuations, genetic perturbations, or gene expression noise.[1–4] Organs initiate at well-defined positions, growing to a robust final size and shape, which is crucial for fitness.[2] For example, the pair of wings in *Drosophila* develop to robust, precisely coordinated final size and shape, which is required for flight.[5–8] The robust positioning of leaves around the stem, phyllotaxis, ensures optimal light capture.[9–11] Whereas these examples of developmental robustness have been well documented, the underlying molecular mechanisms have just begun to be unveiled.

Earlier studies looking for genes involved in maintaining robustness identified *HEAT SHOCK PROTEIN 90* (*HSP90*). The severity of *hsp90* mutant phenotypes varies between individuals, and even between different parts of the same individual, indicating that developmental robustness is disrupted.[3,12,13] *HSP90* encodes a protein chaperone with numerous clients.[3] Mutation of such a hub gene in the gene network thus has broad impacts.[2] Similarly, genes involved in central cellular processes such as chromatin remodeling,[14–16] transcription,[14,15] translation,[17,18] and protein degradation[19,20] are also hub genes important for developmental robustness in various organisms. How these broad-acting hub genes contribute to the robustness of tissue-specific developmental phenotypes remains largely unclear.

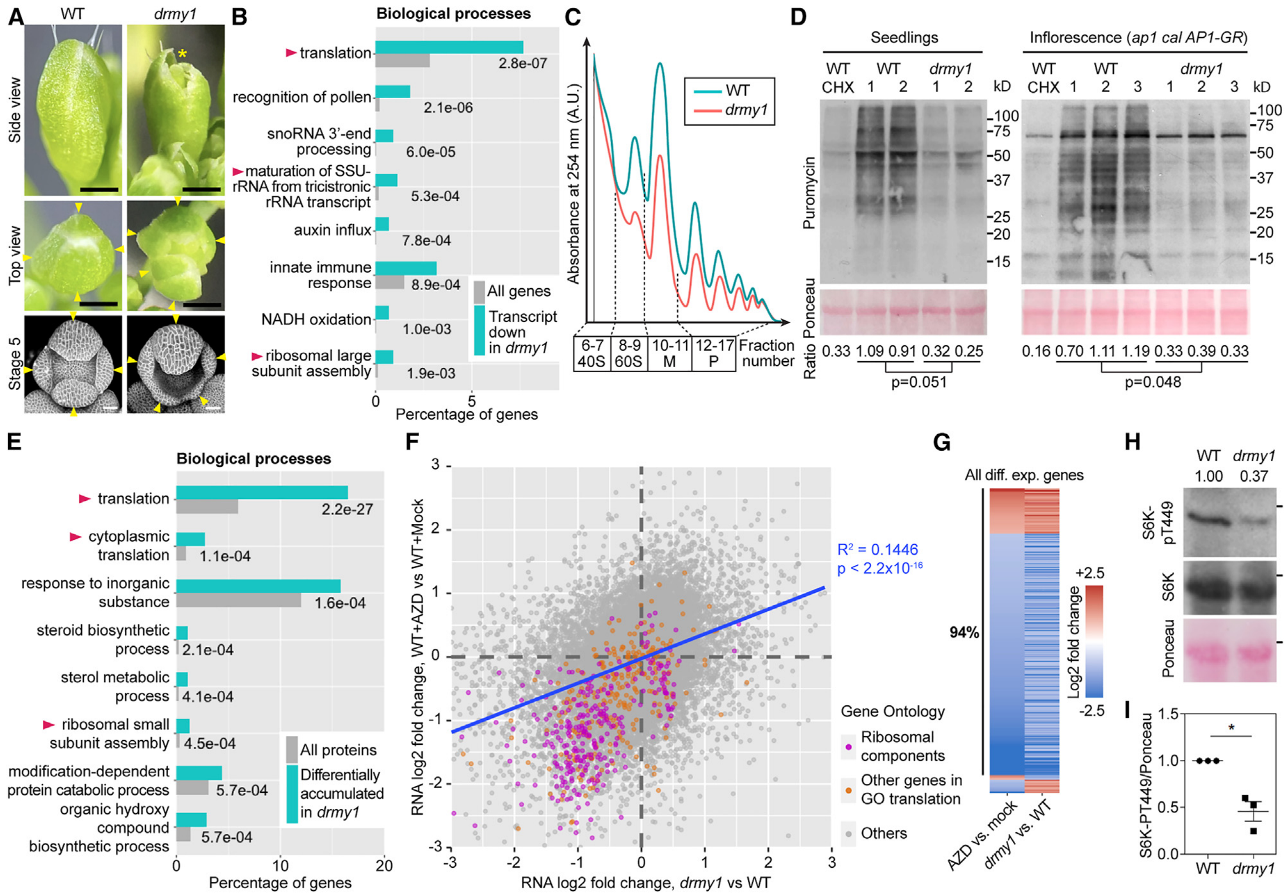

Figure 1. *drmy1* has reduced ribosome abundance, translation rate, and TOR activity

(A) Top row, side view of stage 12 buds. Asterisk shows the gap between sepals. Middle row, top view of stage 12 buds. Arrowheads show sepals. Scale bars, 0.5 mm. Note that *drmy1* has 5 sepals of unequal size, unevenly spaced. Bottom row, stage 5 buds. Arrowheads show sepal primordia. Scale bars, 25 μm.

(B) Top 8 GO terms and their enrichment *p* values for downregulated genes in inflorescences of *drmy1* vs. WT in *ap1 cal AP1-GR* background. See Data S1. Arrowheads highlight terms related to ribosome biogenesis or translation.

(C) Polysomal profiles of WT (blue) and *drmy1* (red) inflorescences in *ap1 cal AP1-GR* background. *n* = 3. Additional replicates are in Data S2. M, monosomes; P, polysomes.

(D) Puromycin labeling of WT vs. *drmy1*. Left, seedling samples. From left to right: WT pre-treated with CHX, two bio-reps of WT pre-treated with mock, and two bio-reps of *drmy1* pre-treated with mock. For seedlings to match in size, WT seedlings were 8 days old and *drmy1* seedlings were 10 days old. Right, inflorescence samples of *ap1 cal AP1-GR* background. From left to right: WT treated with CHX, three bio-reps of WT, and three bio-reps of *drmy1*. Loading control (bottom): Ponceau S-stained RuBisCO large subunit. Ratio: between puromycin and Ponceau S signals, normalized by the mean of WT (*p* values are from two-sided Student's t test).

(E) Top 8 GO terms and their enrichment *p* values of differentially accumulated proteins in inflorescences of *drmy1* vs. WT in *ap1 cal AP1-GR* background. See Data S1. Arrowheads highlight terms related to ribosome biogenesis or translation.

(F and G) Coherent alteration of gene expression by *drmy1* and TOR inhibition. (F) Scatterplot of RNA $\log_2$ fold change in *drmy1* vs. WT (x axis), and WT + AZD-8055 vs. WT + mock (y axis), in 8-day-old seedlings. Genes are color coded: genes in "structural constituents of the ribosome" (GO:0003735) and its offspring terms (magenta); all other genes in translation (GO:0006412) and its offspring terms (orange); all other genes (gray). Blue line shows a linear regression of all points ($R^2 = 0.1446$, $p < 2.2 \times 10^{-16}$). (G) Of the 466 genes differentially expressed under both conditions, 439 (94%) are coherently regulated.

(H and I) Phosphorylation of the direct TOR substrate, S6K-pT449, in 8-day-old seedlings. (H) Top, S6K-pT449. Middle, total S6K protein. Bottom, Ponceau S staining. Dashes, 55 kDa marker. Ratio between S6K-pT449 and Ponceau S signals normalized by WT, quantified in three experiments (I), shows that TOR activity decreased by half in *drmy1* (mean ± SD; *$p < 0.05$).

See also Figure S1 and Data S1, S2, and S3.

The *Arabidopsis* sepal is a system to elucidate the mechanisms of developmental robustness.[21–25] The four sepals of a flower initiate at orthogonal positions and grow to a constant size and shape, allowing them to enclose and protect the developing reproductive organs (Figure 1A). Such robustness stems from the robust initiation of the four sepal primordia from the floral meristem[23] (Figure 1A), which trades off with developmental speed.[25] The sepals attain robust final size and shape by spatiotemporal averaging of cellular growth variability and synchronous progression of a growth termination signal from tip to base.[21] In addition, noise in gene expression must be kept low to ensure sepal size robustness.[26] We previously characterized the *development-related myb-like 1* (*drmy1*) mutant.[23,25] A *drmy1* flower develops 3–5 sepals, often mispositioned and variably sized, leaving gaps in the bud (Figure 1A). This variability in the mature sepal phenotype originates during sepal initiation (Figure 1A, bottom), driven by the loss of robust patterning of auxin and cytokinin,[23] two plant hormones critical for morphogenesis.[27–29] However, how DRMY1 maintains robust hormone patterning is unknown.

Here, we elucidate a mechanism through which DRMY1 maintains robust hormone patterning and thus robust sepal initiation. Specifically, we find that DRMY1 maintains proper activity of TARGET OF RAPAMYCIN (TOR), a crucial regulator of ribosome level and translation.[30,31] When *DRMY1* is mutated, the levels of *ARABIDOPSIS* RESPONSE REGULATOR7 (ARR7) and *ARABIDOPSIS* HISTIDINE PHOSPHOTRANSFER PROTEIN 6 (AHP6), two cytokinin inhibitor proteins, are drastically reduced. Consequently, cytokinin signaling uniformly increases in the floral meristem periphery, causing variability in auxin patterning and sepal initiation. Increasing cytokinin signaling may be a survival mechanism to alleviate reduced translation when ribosomal content is limited. In summary, our work shows that the hub processes of TOR signaling and translation, which occur ubiquitously, have tissue-specific roles in maintaining robust organogenesis by sustaining the rapid synthesis of hormone signaling proteins.

RESULTS

The *drmy1* mutant has reduced TOR activity, ribosome content, and translation rate

DRMY1 encodes a MYB/SANT domain protein that may exert transcriptional regulation.[23] To look for differentially expressed genes in *drmy1* that may be candidates underlying variable sepal initiation, we performed RNA sequencing (RNA-seq) in *drmy1* and wild-type (WT) inflorescences with flowers initiating sepal primordia (*apetala1 cauliflower AP1-GR*; Figure S1A).[32–34] We detected transcripts from a total of 21,496 genes of which 1,042 (4.8%) were differentially expressed in *drmy1* (Figure S1B; Data S1). The 443 genes downregulated in *drmy1* were enriched in the Gene Ontology (GO) term ‘‘translation’’ and several other ribosome-related GO terms (Figure 1B). Within translation, genes encoding ribosomal components were most downregulated (Figure S1C). We therefore hypothesized that ribosomal abundance and translation are affected in *drmy1*, potentially altering the accumulation of proteins critical for developmental robustness.

To determine whether ribosomal abundance is affected in *drmy1*, we performed polysome profiling. All peaks corresponding to 40S, 60S, monosomes, and polysomes were drastically reduced in *drmy1* (Figure 1C; Data S2). To see whether this reduction in ribosomal content affected the *de novo* protein synthesis rate, we performed puromycin labeling.[35,36] In both young seedlings and inflorescences, the puromycin level detected in the *drmy1* mutant was much reduced compared with WT (Figure 1D), indicating a reduction in global translation rate. A reduced global translation rate should result in globally decreased protein levels; a ubiquitously expressed membrane marker *UBQ10::mCherry-RCI2A* had a small ($\sim$25%) but significant decrease in fluorescence intensity in *drmy1* (Figures S1D and S1E). This decrease in fluorescence intensity in *drmy1* is even greater than the decrease in ribosomal mutant *ul4y* (*rpl4d*)[37] (Figures S1F and S1G). Overall, these results show that ribosomal content and translation are indeed reduced in the *drmy1* mutant.

To test how translational reduction in *drmy1* impacts its proteome, we performed proteomics. We identified a total of 5,077 proteins of which 548 (10.8%) were differentially accumulated in *drmy1* (Figure S1B; Data S1). These differentially accumulated proteins were enriched in GO terms related to translation and ribosomes (Figure 1E). Despite a reduction in ribosomal content (Figure 1C), ribosomal component proteins were more abundant in *drmy1* (Figure S1H). Moreover, components of the 26S proteasome were more abundant in *drmy1*, whereas poly(A) binding proteins and tRNA synthetases were less abundant (Data S1). Thus, the machinery responsible for maintaining protein homeostasis is substantially dysregulated in *drmy1*.

TOR is a key regulator of growth-related processes, including ribosome biogenesis and translation.[30,31,38–42] TOR regulates the translation of mRNAs with specific sequence features and increases global protein synthesis by increasing ribosome levels.[31,42–49] We therefore hypothesized that the decrease in ribosomal content and translation in *drmy1* may reflect altered TOR signaling. To test for transcriptomic signatures of TOR inhibition,[31,50,51] we performed RNA-seq on seedlings of WT, *drmy1*, WT treated with AZD-8055 (a potent TOR inhibitor), and mock-treated WT (Data S3). A significant portion of genes differentially expressed under TOR inhibition vs. mock were also differentially expressed in *drmy1* vs. WT (466/2,044 = 22.8%; hypergeometric test, $p = 4.7 \times 10^{-108}$; Figure 1F). Most of these 466 genes were coherently downregulated or upregulated (439/466 = 94.2%, chi-squared test, $p < 2.2 \times 10^{-16}$; Figures 1G and S1I). Genes coherently downregulated were enriched in GO terms related to translation and ribosomes (Figures 1F and S1J). These similar transcriptomic changes support our hypothesis that TOR activity is reduced in *drmy1*. To further test this hypothesis, we measured TOR activity in WT and *drmy1* by assaying the phosphorylation of its direct substrate, RIBOSOMAL PROTEIN eS6 KINASE (S6K).[52,53] S6K phosphorylation drastically decreased in *drmy1*, demonstrating reduced TOR activity (Figures 1H and 1I). Overall, these results suggest that *drmy1* has reduced TOR activity, which decreases ribosomal content and global translation.

Defects in TOR activity, ribosome, and translation disrupt robust sepal initiation

We next asked whether defects in TOR activity, ribosomes, or translation have effects on robust sepal initiation like the *drmy1* mutation does (Figures 2A and 2B).[23] We imaged three ribosomal mutants, *ul4z* (*rpl4a*), *ul4y* (*rpl4d*), and *ul18z* (*rpl5a*),[37] each mutated in a gene that is transcriptionally downregulated in *drmy1* (Figure S1C). The *ul4z* mutant bud showed reduced size of the inner sepal primordia relative to the outer sepal primordia (Figure 2C) and slightly more variable positioning of sepal primordia (Figures 2I and 2J), although it always developed four sepal primordia (Figure 2H). This is a weaker phenotype than *drmy1* but has similar characteristics. The *ul4y* and *ul18z* mutants showed great variability in the number and position of sepal primordia (Figures 2D, 2E, 2H, and 2J), more similar to *drmy1*. In double mutants of *drmy1* and these ribosomal mutants, we observed some buds with more extreme phenotypes than either

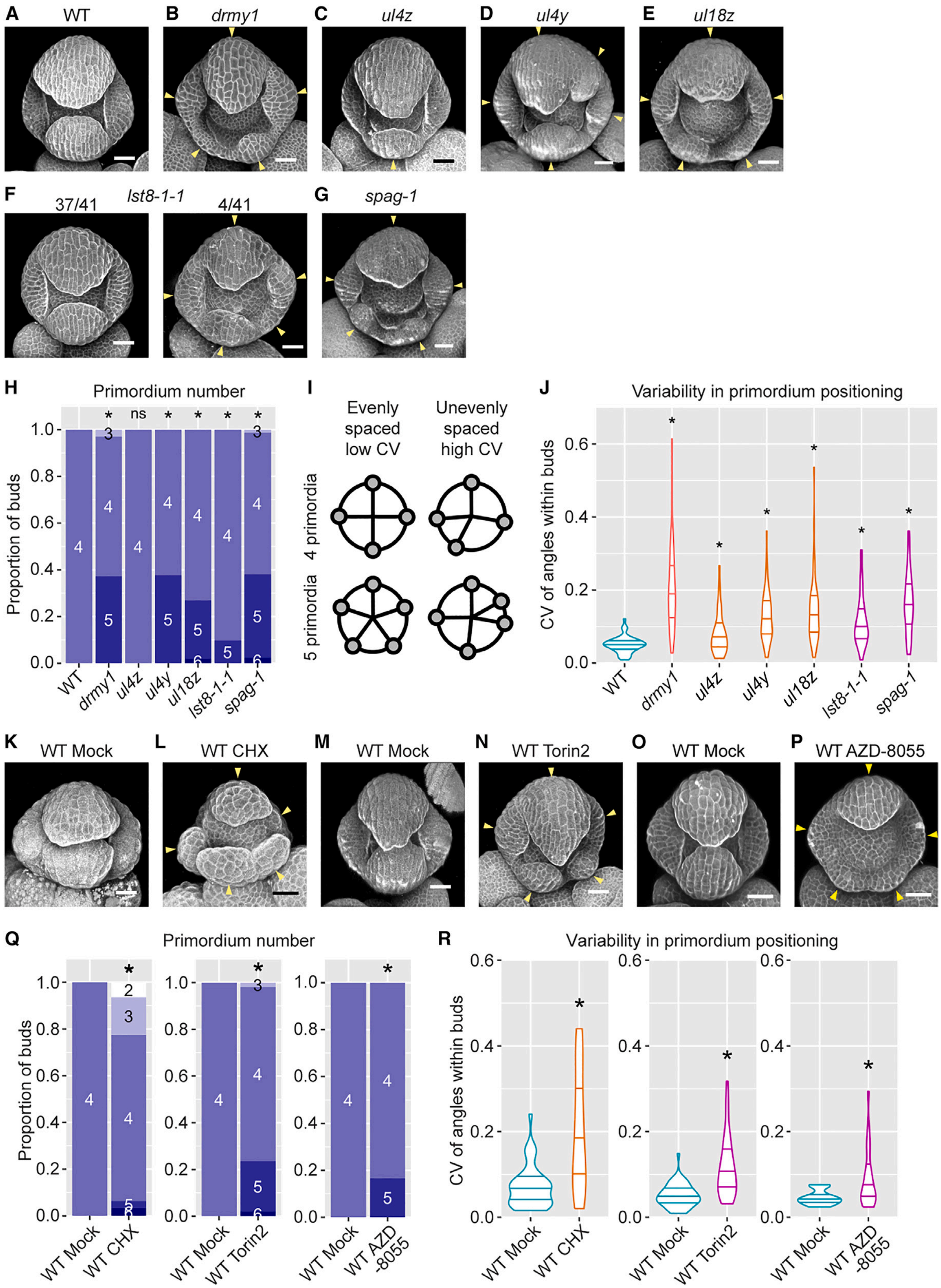

Figure 2. Defects in TOR activity, ribosome, and translation disrupt robust sepal initiation

(A–G) Stage 5 buds. Tissue morphology is visualized by a *35S::mCitrine-RCI2A* membrane marker (A) and (B) or propidium iodide stain (C)–(G). Arrowheads indicate sepal primordia that are variable in number, position, and size (same for K–P).

(legend continued on next page)

single mutant (Figures S2A–S2H), although, on average, sepal initiation was as variable as in the *drmy1* single mutant (Figures S2I and S2J). Homozygous *drmy1 ul18z* double mutants were embryo lethal (Figure S2K), supporting the idea that ribosomal mutations enhance the *drmy1* phenotype.

We then imaged mutants with reduced TOR activity to determine whether sepal initiation is also less robust. *lst8-1-1* is a mutant of a TOR complex (TORC) component[54] and is weakly hypomorphic in TOR activity. We found that *lst8-1-1* showed variable sepal initiation in a small proportion of buds (4/41, 9.8%) (Figures 2F, 2H, and 2J). The *spaghetti-1* mutant, defective in TOR complex 1 (TORC1) assembly,[55] showed a level of variability comparable to the *drmy1* mutant and the ribosomal mutants *ul4y* and *ul18z* (Figures 2G, 2H, and 2J). Mutants with more severe disruption of TOR activity were embryo lethal and could not be analyzed.[55,56] These results show that reduction in TOR activity can cause variability in sepal initiation, similar to *drmy1*.

To corroborate these findings, we inhibited translation by *in vitro* culture of WT inflorescences on 2 μM cycloheximide (CHX). This concentration does not completely block translation. CHX-treated inflorescences developed buds that have 2–6 unevenly spaced sepal primordia with variable sizes (Figures 2K, 2L, 2Q, and 2R). These phenotypes were stronger than *drmy1*. Similarly, we inhibited TOR activity by application of 100 μM Torin2 or 3.2 μM AZD-8055 to the growing shoot apex and we observed variable sepal initiation (Figures 2M–2R). Overall, these data show that inhibition of TOR activity and translation can disrupt the robustness of sepal initiation.

We previously showed that *drmy1* buds develop sepals of different sizes because of increased differences in the initiation timing of sepal primordia within the same bud.[23] We asked whether TOR or ribosomal defects similarly disrupt the relative timing of sepal initiation. In *ul4y*, the time between sepal initiation within a bud was longer than that in WT, and these time differences were more variable across buds, indicating a loss of robustness in organ initiation timing (Figures 3A–3C). Torin2 treatment on WT buds caused similar defects (Figures 3D–3F). These results show that TOR and ribosomal defects can disrupt the precisely orchestrated initiation timing of sepal primordia within the same bud. In *drmy1*, variability in initiation timing causes variable sizes and gaps in mature sepals.[23] In contrast, in *ul4z*, *ul4y*, *ul18z*, and *lst8-1-1*, sepals within the same flower developed to the same mature length, leaving no (*ul4z*, *ul4y*, or *ul18z*) or small gaps (*lst8-1-1*) (Figures S3A–S3N). Sepals that initiated late, grew faster to catch up with the other sepals and closed the gap (Figures S3O–S3Q). Our results suggest that there exists a size-coordinating mechanism—which is independent of TOR or ribosomal functions but requires DRMY1—that allows sepals within the same bud to reach the same mature length. Such a mechanism requires further investigation.

Inhibition of TOR activity and translation increases cytokinin signaling and disrupts the robust spatial pattern of auxin and cytokinin signaling

Auxin and cytokinin are plant hormones critical to development,[27–29] acting synergistically in the shoot apical meristem to promote lateral organ initiation.[11,57,58] Prior to sepal initiation, auxin and cytokinin signaling concentrates at the four incipient primordia, which is required for robust sepal initiation from these regions (Figures 4A and S4A).[23] In the *drmy1* mutant, cytokinin signaling becomes stronger and diffuse around the bud periphery (Figures 4A and 4B). Auxin signaling also becomes more diffuse, forming irregular auxin maxima that are less focused than those in WT, except at the incipient outer sepal where it remains robust (Figures 4A and S4B).[23] These changes in hormone signaling correlate with variable sepal initiation (Figure S4B).[23] We wondered whether ribosomal mutations have similar effects on auxin and cytokinin signaling. We imaged the auxin-signaling reporter *DR5::3xVENUS-N7* and the cytokinin-signaling reporter *TCS::GFP* in floral meristems of the ribosomal mutant *ul4y*. Both reporters lost their robust spatial pattern, except in the incipient outer sepal (Figures 4A and S4C). WT buds showed four clear DR5 and TCS peaks, with very little signal in between, whereas in *drmy1* and *ul4y* there was greater noise and variation all around the bud (Figures 4C and 4D). Diffuse bands of auxin signaling that typically occurred in the adaxial or lateral periphery of *drmy1* and *ul4y* buds later resolved into several distinct auxin maxima at various positions, correlated with the initiation of sepal primordia at these positions (Figures S4B and S4C).

We also tested whether drug treatments that inhibit TOR activity or translation can disrupt the robust hormone patterning. Buds treated *in vitro* with the translation inhibitor CHX (2 μM) for 3 days showed a 50% increase in cytokinin signaling, and both auxin and cytokinin signaling became diffuse around the bud periphery (Figures 4E–4H). By day 6, cytokinin signaling was still diffuse and had doubled in total intensity (Figures 4I, 4J, and 4L). Auxin signaling formed maxima of variable number at variable positions (Figures 4I arrowheads and 4K), correlated with the variable initiation of sepal outgrowth at these positions (Figures S4D and S4E). Similar changes in hormone patterning occurred in buds treated *in vitro* with the TOR inhibitor

(H) Sepal primordium number, comparing *drmy1* (n = 67 buds), *ul4z* (n = 52 buds), *ul4y* (n = 53 buds), *ul18z* (n = 52 buds), *lst8-1-1* (n = 41 buds), and *spaghetti-1* (n = 84 buds) with WT (n = 51 buds). $^*p < 0.05$ in Fisher's contingency table tests compared with WT.

(I) Illustration of robust vs. variable positioning of sepal primordia. Primordia are considered robustly positioned if they are evenly distributed around the bud periphery. Within each bud, angles between adjacent primordia with respect to the bud center are measured, and coefficient of variation (CV) is calculated.

(J) Variability in primordium positioning (CV), following illustration in (I). $^*p < 0.05$ in Wilcoxon's rank sum tests compared with WT.

(K and L) Buds treated *in vitro* with mock (K) or 2 μM CHX (L) for 9–10 days.

(M and N) Buds treated *in planta* with mock (M) or 100 μM Torin2 (N) for 15 days.

(O and P) Buds treated *in planta* with mock (O) or 3.2 μM AZD-8055 (P) for 15 days.

(Q and R) Sepal primordium number (Q) and positional variability (R). Sample size: mock for CHX, n = 42 buds; CHX, n = 31 buds; mock for Torin2, n = 56 buds; Torin2, n = 51 buds; mock for AZD-8055, n = 27 buds; AZD-8055, n = 24 buds.

$^*p < 0.05$ in Fisher's contingency table tests (Q) or Wilcoxon's rank sum tests (R) compared with mock.

Scale bars, 25 μm.

See also Figure S2 and Data S4.

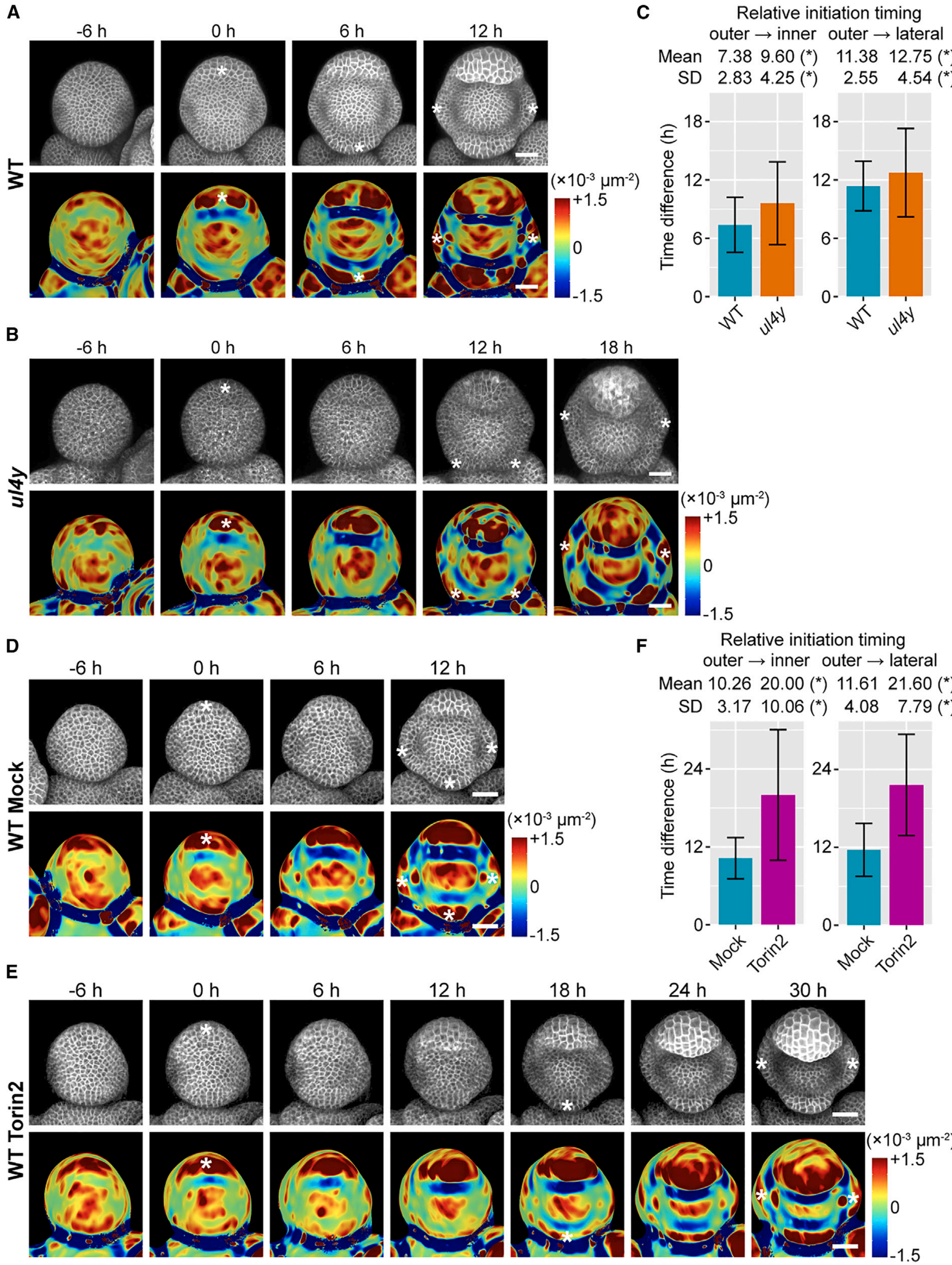

Figure 3. TOR and ribosomal defects cause variability in sepal initiation timing

(A–C) Live imaging of sepal initiation in WT (A, n = 48 buds) and *ul4y* (B, n = 40), quantified in (C).

(D–F) Live imaging of sepal initiation in buds treated *in planta* with mock (D, n = 31) or 100 μM Torin2 (E, n = 15), quantified in (F).

(legend continued on next page)

AZD-8055 (2 μM) for 6 days (Figures 4I–4L). Buds treated *in planta* with 3.2 μM AZD-8055 or 100 μM Torin2 for 15 days showed similar changes, although to a lesser extent (Figures S4F–S4M). Overall, these results suggest that defects in TOR activity and translation cause hormone patterning changes similar to the *drmy1* mutant: an increase in cytokinin-signaling level and a loss of the precise spatial patterning of cytokinin and auxin signaling required for robust sepal initiation.

An increase in cytokinin signaling is necessary and sufficient for variable auxin signaling and sepal initiation under translation inhibition

We wondered what caused auxin to lose its robust patterning during inhibition of TOR activity and translation. It was previously reported that the ribosomal mutants *ul4y*, *ul18z*, and *el24y* have reduced protein levels of AUXIN RESPONSE FACTOR (ARF) 3, 5, and 7,[59–61] key transcription factors that mediate the auxin-signaling response,[62] because they contain upstream open reading frames (uORFs) requiring translation reinitiation.[59–61,63,64] We therefore tested translation of uORF-containing transcripts in *drmy1*. We found a small but significant decrease in the protein-transcript ratio in *drmy1* for the 724 genes containing at least 2 uORFs in their transcripts, supporting the hypothesis that *drmy1* has reduced translation reinitiation for uORF-containing transcripts (Figure S5A; uORF data from Von Arnim et al.[64]). Surprisingly, we saw no correlation between the presence of uORFs and decrease in fluorescent intensity of ARF reporters in *drmy1* (Figures S5B–S5D). This result suggests that the decrease in translation reinitiation of uORF-containing ARFs is not the main factor explaining the loss of robust auxin-signaling pattern in *drmy1*.

External application of cytokinin increases auxin biosynthesis[65] and changes the expression and polarity of PIN-FORMED (PIN) polar auxin transport carriers.[66,67] We previously noticed that external application of 6-benzylaminopurine (BAP), a synthetic cytokinin, induced additional convergence points of PIN1 and increased variability in auxin signaling, causing variability in sepal initiation.[23] Here, we confirmed that whereas the mock-treated WT buds showed four clear peaks of DR5 signal with very little signal in between (Figures 5A and 5B), those treated with BAP showed a less robust spatial pattern, with less distinguishable peaks and larger variation (Figures 5C and 5D). Thus, excessive cytokinin is sufficient for the variable spatial pattern of auxin signaling.

We then wondered whether an increase in cytokinin signaling (Figure 4) was the cause of the variable pattern of auxin signaling under translation-limited conditions such as *drmy1*. To test this hypothesis, we introduced mutations in B-type *ARABIDOPSIS RESPONSE REGULATORS* (*ARRs*) and in a cytokinin receptor *WOODEN LEG* (*WOL*)/*ARABIDOPSIS HISTIDINE KINASE 4* (*AHK4*) into *drmy1* to see whether they rescue the variability in auxin patterning and sepal initiation. Although buds of *arr1,10,12* and *wol* did not show apparent phenotypic differences from WT, *drmy1 arr1,10,12* and *drmy1 wol* largely rescued the *drmy1* phenotype, with much less variability in sepal number, position, and size (Figures 5E–5G and S6). Although the auxin-signaling reporter DR5 was diffuse and variable in *drmy1*, except in the incipient outer sepal (Figures 5H and 5I), in *drmy1 arr1,10,12*, it was focused in all the four incipient sepals that were robustly positioned (Figures 5J and 5K). These results indicate that cytokinin signaling is required for the increased variability in auxin signaling and sepal initiation patterns in *drmy1*.

The translation inhibitor CHX disrupted robustness in auxin signaling and sepal initiation in WT (Figures 2L, 4E, and 4I). We tested whether these effects were still present in *arr1,10,12* and *wol* mutants. Unlike WT, sepal initiation remained mostly robust in *arr1,10,12* and *wol* after 2 μM CHX treatment (Figures 5L–5N). Whereas DR5 in WT became diffuse and occurred in variable positions after 3 days of CHX treatment (Figures 5O and 5P, arrow), DR5 in *arr1,10,12* remained robust and concentrated at the four incipient sepal primordia (Figures 5Q and 5R). These results suggest that an elevated cytokinin-signaling level is the primary cause for variability in auxin patterning under translation-inhibited conditions. Thus, maintaining a low level and focused cytokinin signaling is crucial for robust auxin patterning and sepal initiation.

Upregulation of cytokinin signaling is required to sustain translation and fitness in *drmy1*

Under translation-inhibited conditions, why does the plant upregulate cytokinin signaling at the cost of developmental robustness? Previous studies revealed that cytokinin signaling can stimulate translation.[68–76] We therefore hypothesized that an increase in cytokinin signaling under translation-inhibited conditions (such as *drmy1*) sustains a survivable rate of translation in a feedback loop. We first validated that increased cytokinin signaling (*arr1 35S::ARR1*) increased global translation (Figure 6A; see also Karunadasa et al.[68]) in 14-day-old seedlings. We then tested whether cytokinin signaling is required to sustain global translation (Figures 6B and 6C). Compared with WT, the cytokinin receptor single mutant *wol* had a mild reduction in global translation rate at day 8 and a ∼50% reduction at day 14. The *drmy1* single mutant showed a drastically reduced global translation rate at day 8, but, by day 14, the global translation rate in *drmy1* increased and matched WT. In the *drmy1 wol* double mutant, however, the translation rate was unable to recover at day 14 and remained lower than *drmy1*. Our data suggest that, in *drmy1* plants, the upregulated cytokinin signaling is required to sustain global translation at near-WT levels.

We then hypothesized that an upregulation of cytokinin signaling and the consequent restoration of global translation would benefit fitness in *drmy1*. Thus, we expect that mutation of the cytokinin receptor WOL in *drmy1*, and the consequent failure to sustain global translation, should affect plant vitality and reproduction. We found that, at day 14, the *drmy1* single mutant was slightly smaller than WT, whereas *drmy1 wol* plants were

In (A), (B), (D), and (E), top rows show the *35S::mCitrine-RCI2A* membrane marker, and bottom rows show Gaussian curvature heatmaps of the same images. Asterisks indicate sepal initiation (a primordium with positive curvature adjacent to boundary with negative curvature). Scale bars, 25 μm. (C) and (F) show the time between outer and inner sepal initiation (left) and between outer and lateral sepal initiation (right) within each bud. Bar plot shows mean ± SD. *$p < 0.05$ in Wilcoxon's rank sum test (for mean) or Levene's test (for SD).
See also Figure S3 and Data S4.

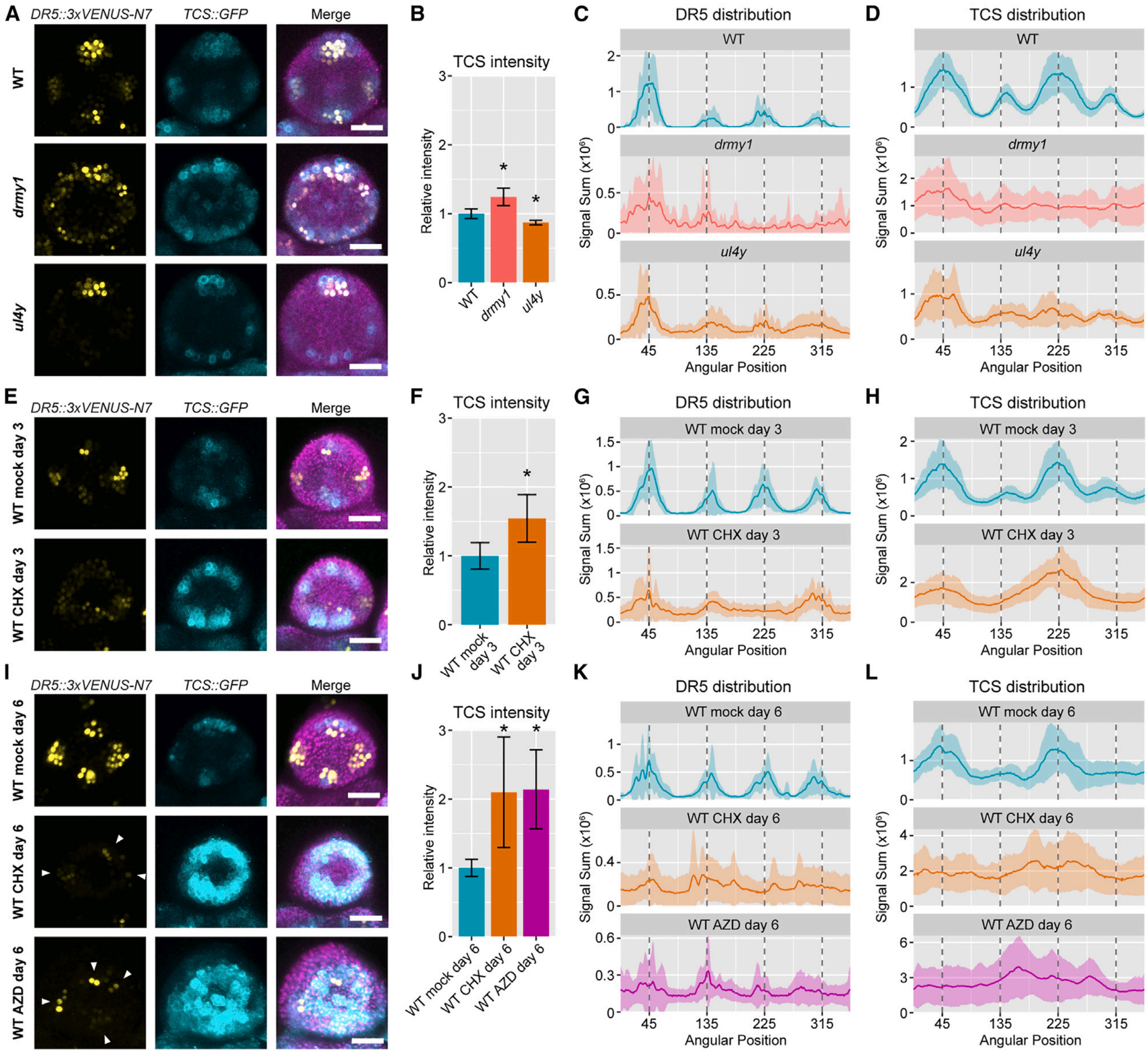

Figure 4. Inhibition of TOR activity and translation cause variability in auxin and cytokinin signaling

(A–D) The ribosomal mutant *ul4y* loses robustness in auxin and cytokinin signaling.

(A) Stage 2 buds of WT, *drmy1*, and *ul4y*, showing the auxin-signaling reporter *DR5::3xVENUS-N7* in yellow, the cytokinin-signaling reporter *TCS::GFP* in cyan, and both merged with chlorophyll (in WT) or *UBQ10::mCherry-RCI2A* (in *drmy1* and *ul4y*) in magenta.

(B) TCS intensity (mean ± SD) normalized to mean of WT. *Two-tailed Student's t tests (*drmy1*, $p = 2.1 \times 10^{-6}$; *ul4y*, $p = 3.4 \times 10^{-5}$).

(C and D) Circular histograms of DR5 and TCS signal distribution. In WT, the incipient outer sepal is near 45°, the incipient inner sepal near 225°, and the incipient lateral sepals near 45° and 135° (vertical dotted lines). Solid line represents mean, and shaded area represents mean ± SD. WT, $n = 12$ buds; *drmy1*, $n = 15$ buds; *ul4y*, $n = 10$ buds.

(E–H) 3 days of translation inhibition causes increased and diffuse cytokinin signaling and diffuse auxin signaling. (E) WT buds treated *in vitro* with mock or 2 μM CHX for 3 days. (F) TCS intensity. *Two-tailed Student's t test ($p = 2.0 \times 10^{-4}$). (G) and (H), circular histograms of DR5 and TCS. Mock, $n = 10$ buds; CHX, $n = 12$ buds.

(I–L) 6 days of TOR or translation inhibition causes increased and diffuse cytokinin signaling, and randomly positioned auxin-signaling maxima. (I) WT buds treated *in vitro* with mock, 2 μM CHX, or 2 μM AZD-8055 for 6 days. Arrowheads show randomly positioned auxin maxima. (J) TCS intensity. *Two-tailed Student's t tests (CHX, $p = 1.0 \times 10^{-3}$; AZD-8055, $p = 1.2 \times 10^{-4}$). (K) and (L), circular histograms of DR5 and TCS. Mock, $n = 12$ buds; CHX, $n = 11$ buds; AZD-8055, $n = 10$ buds. Scale bars, 25 μm.

See also Figure S4 and Data S4.

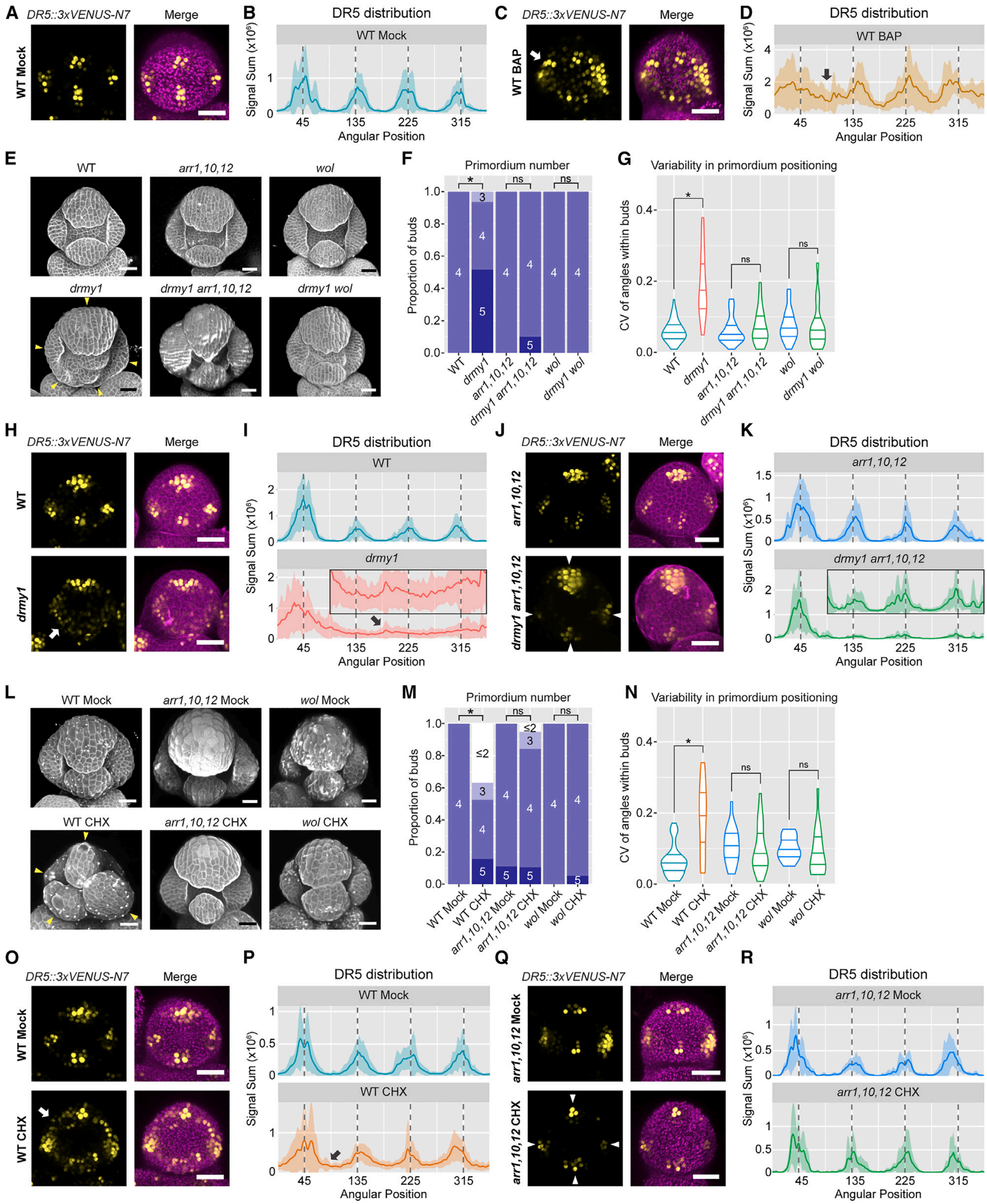

Figure 5. Cytokinin signaling is required for increased variability in auxin signaling and sepal initiation under translation inhibition

(A–D) Cytokinin treatment makes auxin signaling diffuse. Shown are WT buds under mock (A) and (B) or 5 μM cytokinin (BAP) treatment (C) and (D) for 4 days. (A) and (C) auxin-signaling reporter *DR5* in yellow, and *DR5* merged with chlorophyll in magenta. (B) and (D) Circular histograms (mean ± SD). Arrows show DR5 signal in variable positions. n = 10 buds each.

(legend continued on next page)

extremely retarded compared with *wol*, with tiny and chlorotic cotyledons and leaves (Figure 6D). In older plants, the *drmy1* single mutant had similar rosette size and slightly shorter inflorescences compared with WT. In contrast, *drmy1 wol* produced tiny rosettes and stunted inflorescences, with a few chlorotic buds that developed into short siliques (Figures 6E and S6F). Similarly, growth of *drmy1 arr1,10,12* was much retarded compared with *arr1,10,12* (Figures 6F and S6E) and all seeds had aborted in the siliques (Figure 6G). Although it remains possible that unknown effects of the cytokinin-signaling pathway other than promoting translation are critical for the vitality of *drmy1*, the data are consistent with our hypothesis that the upregulation of global translation (Figure 6A) by increased cytokinin signaling (Figure 4) maintains a survivable level of protein synthesis in plants with reduced ribosomal content, such as *drmy1*.

TOR and translation inhibition decreases the protein level of cytokinin-signaling inhibitors ARR7 and AHP6

What causes cytokinin signaling to increase in plants with reduced TOR activity and translation? We first tested whether *drmy1* has more cytokinin levels than WT; however, we found no significant difference in the levels of *trans*-Zeatin, *cis*-Zeatin, isopentenyladenine, and their nucleosides (Figure S7A). Also, the transcript levels of most cytokinin-signaling components did not significantly differ between *drmy1* and WT (Figure S7B). These results suggest that TOR and translation inhibition increases cytokinin signaling through post-transcriptional regulations, including protein synthesis.

We considered the effects that a decrease in global translation might have on the protein components of the cytokinin-signaling pathway. In particular, A-type *ARR*s, which encode inhibitors of cytokinin signaling,[77–79] are rapidly induced upon cytokinin application to dampen cytokinin response.[80–82] Likewise, *AHP6* is highly expressed in lateral organ primordia downstream of auxin signaling, which non-cell-autonomously represses and restricts cytokinin signaling to robust spatial patterns.[11] The rapid synthesis of the A-type ARR and AHP6 proteins may be crucial for maintaining the homeostasis of cytokinin signaling during development. We therefore hypothesized that translation defects in *drmy1* may cause reduced synthesis of these proteins, decreasing them to a level insufficient to repress cytokinin signaling (Figure 7A).

To visualize A-type ARR proteins, we employed LlamaTag, a recently developed method to visualize the abundance of nuclear-localized proteins with short half-lives.[83] We used LlamaTag because we were unable to detect fluorescence in the inflorescence of a traditional GFP fusion (*pARR4::ARR4-GFP*[84]) and A-type ARRs have low protein levels (not detected in our proteomics dataset) and short half-lives.[85] We focused on ARR7, the most highly expressed A-type ARR in our inflorescence RNA-seq (Figure S7B), which is nuclear localized.[86,87] ARR7 was fused to a fast-folding, anti-GFP LlamaTag (ARR7-llama). Soon after translation, the fusion binds cytoplasm-localized GFP (GFP-nes, with a nuclear exclusion signal) and translocates it to the nucleus. Thus, GFP fluorescence in the nucleus indicates ARR7 abundance (Figures 7B and 7C). Nuclear GFP signal in *ARR7-llama GFP-nes* increased within 5 h of 200 μM BAP treatment (Figures S7C and S7D), consistent with previously reported effect of cytokinin in increasing A-type ARR expression and protein stability.[85,88]

We then compared *ARR7-llama GFP-nes* in floral meristems of WT and *drmy1* before sepal initiation. If increased cytokinin signaling in *drmy1* was at least in part caused by insufficient ARR7 level, we would see reduced nuclear GFP signal in *drmy1 ARR7-llama GFP-nes*. Otherwise, we would see increased ARR7 level and nuclear GFP signal because cytokinin signaling increases the gene expression and protein stability of A-type ARRs.[81,85,88,89] We found that nuclear ARR7 level was reduced in the *drmy1* mutant, particularly in the bud periphery where sepals initiated (Figures 7D and 7E). We next tested whether this conclusion holds in other translation-inhibited conditions. CHX treatment for 24 h drastically reduced the nuclear ARR7 level (Figure 7F). AZD-8055 treatment for 72 h had a milder but similar effect (Figures 7G and S7E–S7H). Thus, conditions that decrease global protein synthesis greatly decrease the nuclear level of ARR7 protein.

We also tested whether TOR or translation inhibition alter the protein level of AHP6. We imaged the *pAHP6::AHP6-VENUS*[11] protein reporter under mock, CHX, or AZD-8055 treatment. Whereas mock-treated buds highly accumulate the AHP6 protein in the four incipient sepal primordia, buds treated with CHX or AZD-8055 abolished AHP6 accumulation within 72 h (Figure 7H). The *pAHP6::GFP-ER*[90] transcriptional reporter did not change under these treatments (Figure 7I), in agreement with our RNA-seq data of WT vs. *drmy1* (Figure S7B), suggesting that the change in AHP6 protein level is due to post-transcriptional regulation such as altered translation.

To determine whether inhibition of TOR and translation also reduces positive regulators of cytokinin signaling, we tested AHP3,

(E–G) Cytokinin signaling is required for variable sepal initiation in *drmy1*. (E) Stage 5 buds. Sepal primordia in *drmy1* are variable (arrowheads), which does not occur in *drmy1 arr1,10,12* and *drmy1 wol*. (F) and (G) Sepal primordium number (F) and positional variability (G), comparing WT (n = 58) vs. *drmy1* (n = 31), *arr1,10,12* (n = 24) vs. *drmy1 arr1,10,12* (n = 20), and *wol* (n = 36) vs. *drmy1 wol* (n = 39). *$p < 0.05$ in Fisher's contingency table tests (F) or Wilcoxon's rank sum tests (G).

(H–K) Cytokinin signaling is required for diffuse auxin signaling in *drmy1*. Shown are stage 2 buds of WT vs. *drmy1* (H) and (I), and *arr1,10,12* vs. *drmy1 arr1,10,12* (J) and (K). Arrows in (H) and (I) show diffuse DR5 signal. Arrowheads in (J) show four robust auxin maxima. (I) and (K), circular histograms of the *DR5* signal. Inset: 90°–360° are enlarged (y axis range 0–0.4). WT, n = 19; *drmy1*, n = 16; *arr1,10,12*, n = 13; *drmy1 arr1,10,12*, n = 9.

(L–N) Cytokinin signaling is required for variable sepal initiation under translation inhibition. (L) Stage 6 buds of WT, *arr1,10,12*, and *wol*, treated with mock or 2 μM CHX for 10 days. (M) and (N) Sepal primordium number (M) and positional variability (N). WT mock, n = 29; WT CHX, n = 19; *arr1,10,12* mock, n = 18; *arr1,10,12* CHX, n = 19; *wol* mock, n = 15; *wol* CHX, n = 19. *$p < 0.05$ in Fisher's contingency table tests (M) or Wilcoxon's rank sum tests (N).

(O–R) Cytokinin signaling is required for diffuse auxin signaling under translation inhibition. Shown are stage 2 buds of WT (O) and (P) and *arr1,10,12* (Q) and (R), treated with mock or 2 μM CHX for 3 days. Arrows in (O) and (P) show diffuse DR5 signal. Arrowheads in (Q) show four robust auxin maxima. (P) and (R) Circular histograms of the *DR5* signal. WT mock, n = 17; WT CHX, n = 18; *arr1,10,12* mock, n = 7; *arr1,10,12* CHX, n = 7.

Scale bars, 25 μm.

See also Figures S5 and S6 and Data S4.

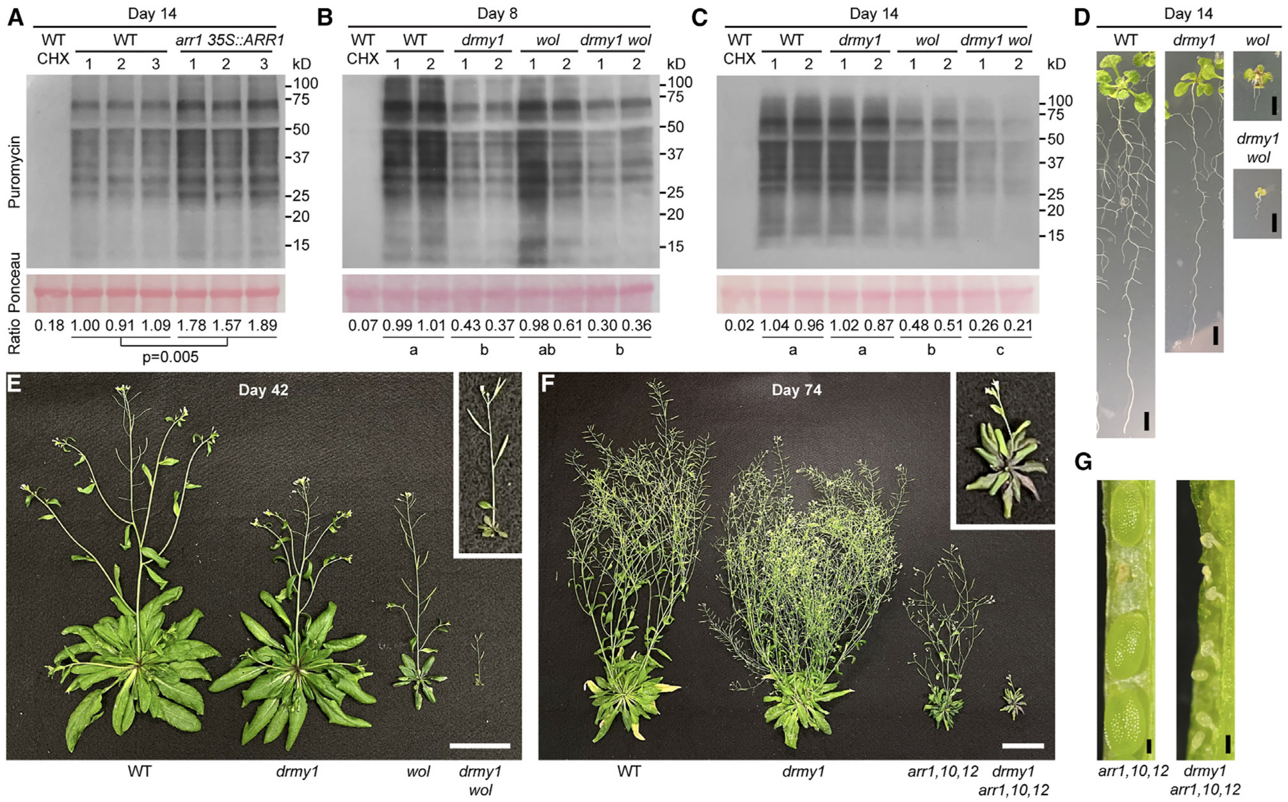

Figure 6. Upregulation of cytokinin signaling is required to maintain translation and fitness in *drmy1*

(A) Puromycin labeling of WT seedlings with 4 h CHX pre-treatment (control), and three bio-reps of WT and *arr1 35S::ARR1* seedlings with 4 h mock pre-treatment.

(B and C) Puromycin labeling of WT seedlings with 4 h CHX pre-treatment (control), and two bio-reps of WT, *drmy1*, *wol*, and *drmy1 wol* seedlings with 4 h mock pre-treatment.

For (A)–(C), age of seedlings is indicated on top. Loading control: RuBisCO large subunit, Ponceau S-stained. Ratio: between puromycin and Ponceau S, normalized to mean of WT. *p* value in (A) is from a two-sided Student's t test. Letters in (B) and (C) show Tukey's pairwise comparison in a one-way ANOVA model.

(D) 14-day-old seedlings of WT, *drmy1*, *wol*, and *drmy1 wol*. Scale bars, 5 mm.

(E) Aerial part of 42-day-old plants of WT, *drmy1*, *wol*, and *drmy1 wol*. Inset shows the magnified *drmy1 wol* plant. Scale bar, 5 cm. See also Figure S6F.

(F) Aerial part of 74-day-old plants of WT, *drmy1*, *arr1*,*10*,*12*, and *drmy1 arr1*,*10*,*12*. Inset shows the magnified *drmy1 arr1*,*10*,*12* plant. Scale bar, 5 cm. See also Figure S6E.

(G) Dissected siliques of *arr1*,*10*,*12* (left) and *drmy1 arr1*,*10*,*12* (right) showing developing seeds. Notice that whereas *arr1*,*10*,*12* occasionally have aborted seeds, all seeds in the *drmy1 arr1*,*10*,*12* silique were aborted. Scale bars, 0.2 mm.

See also Data S4.

a component of the cytokinin phosphorelay.[91,92] CHX treatment did not affect the level or spatial localization pattern of the *pAHP3::AHP3-GFP* reporter,[93] whereas AZD-8055 treatment only mildly decreased its level (Figure S7I). We also tested how the levels of other, more generic proteins respond to TOR and translation inhibition. Unexpectedly, the level of *pUBQ10::mCherry-RCI2A* increased upon 72 h of CHX or AZD-8055 treatments (Figure S7J). Overall, these results show that TOR and translation inhibition does not result in a uniform reduction in the level of all proteins, but specific proteins such as ARR7 and AHP6 are more dramatically decreased. Furthermore, these results are consistent with our hypothesis that depletion of cytokinin-signaling inhibitor proteins, including ARR7 and AHP6, may underlie the upregulation of cytokinin signaling when the floral meristem is under TOR or translation inhibition.

We next tested whether the reduction of A-type ARR or AHP6 proteins contributes to the variability in sepal initiation. High-order mutants of A-type *ARR*s (*arr3,4,5,6,7,8,9,15*[94]) show reduced size of the inner sepal primordium (Figures 7J and 7K) and a minor but significant increase in the positional variability of sepal primordia (Figure 7Q), although sepal primordium number remains robust (Figure 7P). The *ahp6* mutant[11] shows great variability of sepal primordium number, position, and size, although to a lower extent than *drmy1* (Figures 7J, 7L, 7P, and 7Q). Similarly, if the reduction of ARR7 level in *drmy1* contributes to variability in sepal initiation, increasing ARR7 expression should restore sepal initiation robustness. Introducing *ARR7-llama* into *drmy1* plants partially restored robustness in sepal initiation, particularly in the positioning of sepal primordia (Figures 7M–7Q) and sepal size (Figures S7K–S7N). Overall, these results show that reducing the level of cytokinin-signaling inhibitor proteins ARR7 and AHP6 creates variability in sepal primordium initiation, and increasing their level in *drmy1* partially restores robustness. We propose that, during hormone patterning prior to sepal initiation, the rapid synthesis of these inhibitor proteins in response to auxin and cytokinin signaling is crucial for

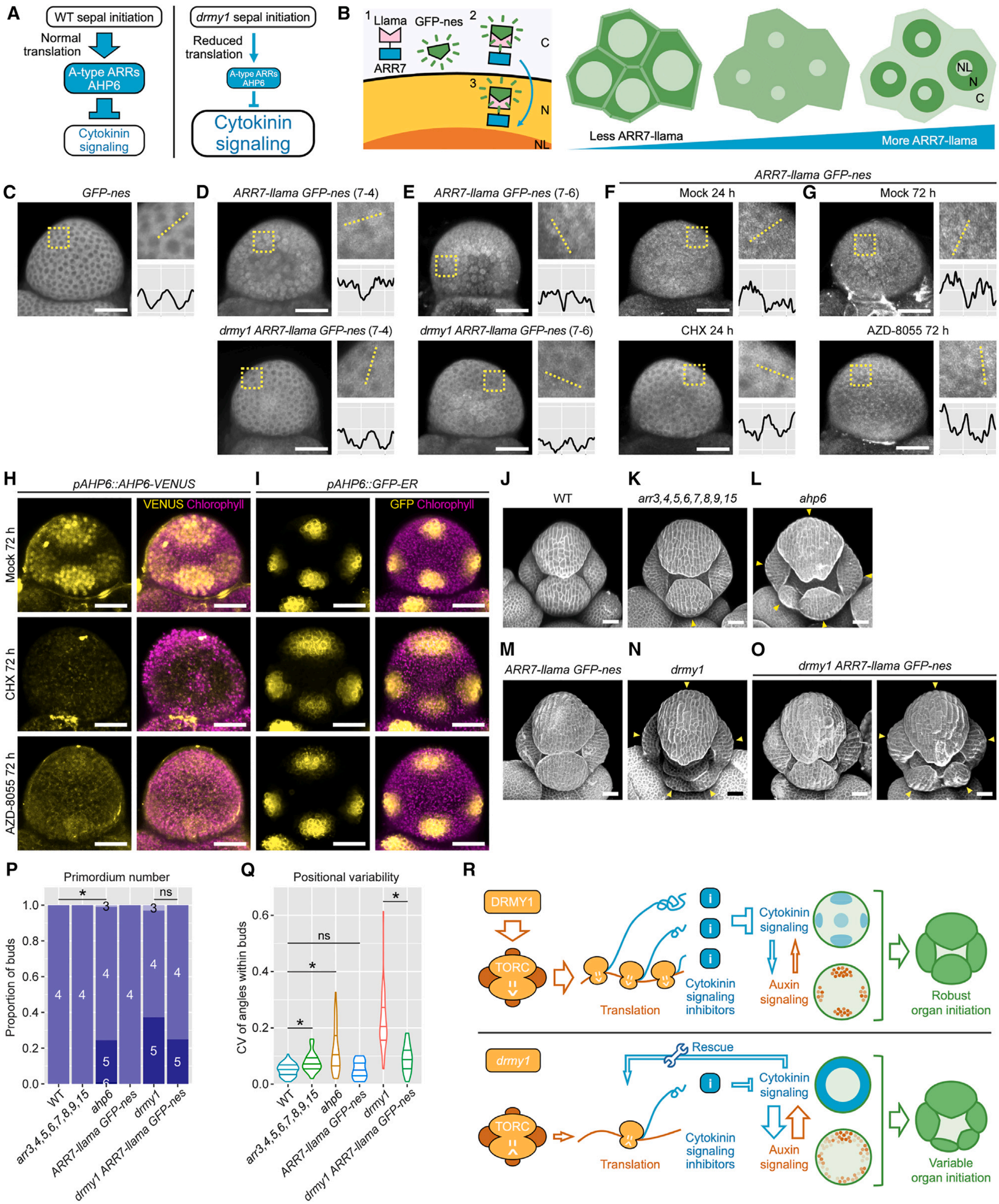

Figure 7. ARR7 and AHP6 protein levels are reduced upon inhibition of TOR and translation

(A) Hypothesis: A-type ARR and AHP6 proteins are rapidly produced to dampen cytokinin signaling to a normal level. In *drmy1*, reduced protein synthesis causes reduced levels of these inhibitor proteins, upregulating cytokinin signaling.

(legend continued on next page)

maintaining the homeostasis of cytokinin signaling and, thus, the robustness in sepal initiation.

We also considered other hormone-related proteins that are dynamically regulated and thus may be depleted under translation defects. AUXIN/INDOLE-3-ACETIC ACID INDUCIBLE (Aux/IAA) proteins are auxin-signaling inhibitors that are rapidly induced by auxin.[95,96] They bind auxin and are rapidly degraded,[97–100] dependent on domain II (DII).[99–101] We hypothesized that the level of Aux/IAAs would be drastically decreased in translation-inhibited conditions because synthesis is unable to keep up with degradation upon auxin signaling. To test this, we used the R2D2 reporter,[102] which contains a DII fused with 3xVENUS (*pUS7Y::DII-n3xVENUS*), and, as a control, a mutated non-degradable DII fused with tdTomato (*pUS7Y::mDII-ntdTomato*). DII-VENUS was not reduced in *drmy1* but instead slightly but significantly elevated (Figures S7O and S7P). Overall, these results suggest that the level of DII-containing Aux/IAA proteins is not reduced in *drmy1*, despite the high requirement for synthesis due to their rapid turnover. Thus, not all proteins that are dynamically regulated in response to hormone signaling are equally affected by translation inhibition.

DISCUSSION

Robustness, the strikingly reproducible development of phenotype, has fascinated biologists for decades.[2] The *Arabidopsis* flower robustly develops four sepals of equal size. This stems from the robust initiation of four sepal primordia from the floral meristem, which is, in turn, dictated by the robust patterning of auxin and cytokinin controlled by DRMY1.[23] Here, we show that DRMY1 sustains TOR activity, ribosomal content, and translation, which controls robust hormone patterning and thus robust sepal initiation. We further show that inhibition of TOR activity or translation is sufficient to cause variability in the initiation timing, position, and number of sepal primordia, mimicking the *drmy1* phenotype. Our findings agree with previous studies that have shown robustness is often maintained by genes involved in central cellular processes.[2] In our case, the rate of translation in WT maintains proper levels of ARR7 and AHP6, two cytokinin-signaling inhibitor proteins, which need to be rapidly synthesized to dampen cytokinin signaling. Homeostasis of cytokinin signaling ensures robustness in auxin-signaling patterns and thus robustness in sepal initiation (Figure 7R, top). In the *drmy1* mutant, reduced TOR activity, ribosomal content, and translation rate prevent rapid synthesis of these inhibitor proteins. Consequently, cytokinin signaling is elevated, disrupting the robust spatial pattern of auxin signaling, leading to variable sepal initiation (Figure 7R, bottom). Blocking cytokinin signaling in *drmy1* is sufficient to restore robust initiation of four sepal primordia but has severe consequences on the overall fitness of the plant. Our results reveal how defects in hub cellular processes such as TOR signaling and translation can have tissue-specific phenotypic effects.

It was discovered long ago that cytokinin application to plant tissue or cell-free extracts can promote translation,[69–72] at least in part mediated by the cytokinin-signaling pathway.[68,76] Here, we show that cytokinin signaling is upregulated in translation-inhibited conditions (Figure 4), which maintains the translation rate at a level necessary for the survival and reproduction of the plant (Figure 6). We propose that this represents a homeostasis mechanism where plants leverage increased cytokinin signaling to rescue reduced translation rate (Figure 7R, bottom).

Although translation-inhibited plants likely upregulate cytokinin signaling to maintain protein synthesis, this upregulation negatively affects developmental robustness. Our results suggest that cytokinin upregulation is necessary and sufficient for variability in auxin patterning and sepal initiation, indicating that the cytokinin-signaling changes are primary defects in

(B) Illustration of LlamaTag. Plants were co-transformed with *ARR7-llama* (*pARR7::ARR7-linker-llama-ARR7ter*) and *GFP-nes* (*pUBQ10::sfGFP-nes-UBQ3ter*). Without ARR7-llama, GFP localizes to the cytosol due to the nuclear export sequence (nes). ARR7-llama is produced in the cytoplasm (C), binds GFP-nes, and translocates into the nucleus (N,excluded from the nucleolus, NL). Thus, the amount of GFP in the nucleus shows ARR7-llama protein level.

(C) *GFP-nes* signal in the cytoplasm.

(D and E) GFP images of buds from two independent lines of *ARR7-llama GFP-nes*, 7-4 (D) and 7-6 (E), of WT (top) vs. *drmy1* (bottom). Images represent $n = 17$ (line 7-4, WT), $n = 40$ (line 7-4, *drmy1*), $n = 9$ (line 7-6, WT), and $n = 6$ (line 7-6, *drmy1*) buds. Note that GFP is more cytoplasm localized in *drmy1*, indicating reduced ARR7-llama protein level.

(F) GFP images of WT *ARR7-llama GFP-nes* buds treated with mock (top, $n = 20$ buds from three independent lines) or 2 μM CHX (bottom, $n = 19$ buds, same lines) for 24 h.

(G) GFP images of WT *ARR7-llama GFP-nes* buds treated with mock (top, $n = 13$ buds from two independent lines) or 2 μM AZD-8055 (bottom, $n = 11$ buds, same lines) for 72 h.

For (C)–(G), each image was brightened to reveal subcellular localization patterns of GFP. GFP intensity was quantified along a line in an enlarged square region containing 5–10 cells. x axis, pixels (0–238). y axis, GFP intensity (smoothened by averaging 11-pixel neighborhoods; range 90–210 in gray value).

(H and I) Response of the AHP6 protein reporter (H) and transcriptional reporter (I) to mock, CHX, and AZD-8055 treatments for 72 h. For (H), images represent $n = 29$ (mock), $n = 29$ (CHX), and $n = 34$ (AZD-8055) buds in three experiments. For (I), images represent $n = 11$ (mock), $n = 9$ (CHX), and $n = 12$ (AZD-8055) buds in two experiments.

(J–Q) Reduction of A-type ARR and AHP6 protein levels contribute to the variability in sepal initiation. (J)–(O), stage 5–6 buds. Arrowheads, variably initiated sepal primordia. The *ARR7-llama GFP-nes* constructs partially rescue the *drmy1* phenotype in some buds (O, left) but not others (O, right). (P) Sepal primordium number. Fisher's exact test (WT vs. *ahp6*, $p = 3.026 \times 10^{-7}$; *drmy1* vs. *drmy1 ARR7-llama GFP-nes*, $p = 0.4389$). (Q) Variability in sepal primordium position. Wilcoxon rank sum test (WT vs. *arr3,4,5,6,7,8,9,15*, $p = 2.948 \times 10^{-4}$; WT vs. *ahp6*, $p = 2.137 \times 10^{-11}$; WT vs. *ARR7-llama GFPnes*, $p = 1$; *drmy1* vs. *drmy1 ARR7-llama GFPnes*, $p = 1.538 \times 10^{-7}$). Data for *drmy1* were reused from Figures 2H and 2J. Data for *ARR7-llama GFP-nes* and *drmy1 ARR7-llama GFP-nes* were pooled from two independent lines (7-4 and 76). WT, $n = 78$; *arr3,4,5,6,7,8,9,15*, $n = 28$; *ahp6*, $n = 106$; *ARR7-llama GFPnes*, $n = 16$; *drmy1*, $n = 67$; *drmy1 ARR7-llama GFP-nes*, $n = 20$.

(R) Working model. DRMY1 maintains TOR activity and translation, which sustains the rapid production of cytokinin-signaling inhibitors (ARR7 and AHP6) necessary for robust patterning of cytokinin and auxin signaling to initiate sepal primordia.

Scale bars, 25 μm.

See also Figure S7 and Data S4.

Please cite this article in press as: Kong et al., DRMY1 promotes robust morphogenesis in *Arabidopsis* by sustaining the translation of cytokinin-signaling inhibitor proteins, Developmental Cell (2024), https://doi.org/10.1016/j.devcel.2024.08.010

drmy1 and the auxin-signaling changes are secondary. Our results suggest a mechanism different from that previously reported, where ribosomal mutations affect auxin signaling through reduced translation reinitiation of uORF-containing mRNAs, including those of ARFs.[59–61] Overall, our results suggest that homeostasis in cytokinin signaling is crucial for maintaining robust patterns of auxin signaling and sepal initiation.

Mutations affecting ribosome abundance or translation have long attracted interest due to the surprisingly tissue-specific phenotypes they cause.[103] In humans, these mutations have been associated with diseases collectively known as ribosomopathies, where patients show abnormalities in a range of organs, and such abnormalities vary between individuals.[104–109] Ribosomal mutants have been characterized in numerous other species, including both animals and plants, with similarly broad and variable impacts.[18,59,61,110–118] We propose that *drmy1* is an *Arabidopsis* ribosomopathy mutant like those previously characterized.

Several mechanisms have been proposed to explain why ribosomopathies do not usually cause a general reduction in growth but rather affect development in tissue-specific ways. These include extra-ribosomal functions of certain ribosomal proteins,[119–123] altered translation behavior of ribosomal variants on certain mRNAs,[124] different competitiveness of mRNAs for scarce ribosomes,[59–61,125–128] and high translation-rate requirement for certain proteins.[129,130] In our case, during lateral organ initiation, ARR7 and AHP6 proteins need to be rapidly produced downstream of cytokinin and auxin signaling, respectively,[131,132] to ensure homeostasis of cytokinin signaling and thus developmental robustness. The ribosomopathy mutant *drmy1* cannot rapidly produce these proteins, disrupting robustness in hormone patterning and sepal initiation. Additionally, *drmy1* shows other phenotypic changes, such as enlarged shoot apical meristem, reduced apical dominance, phyllotaxy defects, and reduced root system, all of which are related to altered cytokinin-/auxin-signaling activity.[23] Thus, our work highlights how downregulation of proteins with high translational requirements can underlie the tissue-specific phenotypes of ribosomopathy.

Limitations of the study

Detailed molecular mechanisms through which DRMY1 maintains TOR signaling remain unknown. DRMY1 contains a MYB/SANT domain[23] and, therefore, could promote TOR signaling by functioning as a transcription factor or chromatin remodeler. Alternatively, DRMY1 could regulate TOR signaling by protein binding. DRMY1 was shown to interact with microspherule protein 1 (MCRS1), whose human ortholog is important for mTORC1 activation on the lysosomal membrane,[133,134] so DRMY1 could promote TOR signaling by interacting with MCRS1 and activating TORC1. These hypotheses demand future studies.

Although we propose that reduced TOR activity and translation affects developmental robustness through reduced synthesis of ARR7 and AHP6, we do not exclude other potential mechanisms that could contribute to the *drmy1* phenotype. For example, several subunits of the 26S proteasome are more abundant in *drmy1* vs. WT (Data S1), which could reflect or influence the accumulation of proteotoxic peptides and disrupt protein homeostasis.[135–139] This accumulation of 26S proteasomes could function upstream and/or downstream of the TOR defect.[31,140–145] Substantial future research is needed to comprehensively define how DRMY1 participates in the complex interactions among TOR, translation, and proteolysis.

RESOURCE AVAILABILITY

Lead contact

Further information and requests for resources and reagents should be directed to and will be fulfilled by the lead contact, Adrienne H.K. Roeder (ahr75@cornell.edu).

Materials availability

Plasmids and seeds generated in this study are available upon request.

Data and code availability

- RNA-seq data have been deposited at NCBI Gene Expression Omnibus (GEO) and BioProject. Mass spectrometry data for proteomics have been deposited at the ProteomeXchange Consortium via the PRIDE[146] partner repository. Mass spectrometry data for cytokinins were deposited in NIH's National Metabolomics Data Repository (NMDR) website, the Metabolomics Workbench.[147] These data are publicly available as of the date of publication. Accession numbers are listed in the key resources table.
- This paper does not report original code.
- Any additional information required to reanalyze the data reported in this paper is available from the lead contact upon request.

ACKNOWLEDGMENTS

We thank Bella Burda, Frances Clark, Byron Rusnak, Erich Schwarz, Avilash Yadav, and Maura Zimmermann for comments on the manuscript. We thank Frank Wellmer, Elliot Meyerowitz, Arnavaz Garda, Teva Vernoux, Géraldine Brunoud, Jan Smalle, Joseph Kieber, Jamie Winshell, Thomas Greb, Min-Hao Chiang, Jianru Zuo, and the Arabidopsis Biological Resource Center for seeds and plasmids. We thank Georg Jander, Brian Curtis, Frank Schroeder, Sheng Zhang, Qin Fu, Vicky Spencer, and Minsung Kim for technical expertise. We thank Richie Ragas, Yanã Rizzieri, and Ziqing Wei for experimental assistance. This research was supported by the National Institute of General Medical Sciences of the National Institutes of Health (NIH) under award numbers R01GM134037 (A.H.K.R.), DP5OD023072 (J.O.B.), and R01GM145814 (J.O.B.); Cornell Graduate School new student fellowship (S.K.); and a Schmittau-Novak Grant from the School of Integrative Plant Science, Cornell University (M.Z.). H.G.G. was supported by NIH Director's New Innovator Award (DP2 OD024541-01), NSF CAREER award (1652236), NIH R01 Award (R01GM139913), and the Koret-UC Berkeley-Tel Aviv University Initiative in Computational Biology and Bioinformatics. H.G.G. is also a Chan Zuckerberg Biohub-San Francisco investigator. We thank the Metabolomics Workbench funded by NIH U2C-DK119886 and OT2-OD030544, the Biotechnology Resource Center (BRC) Genomics Facility (RRID:SCR_021727) and Proteomics Facility (RRID:SCR_021743) of Cornell University (supported by NIH Sig Grant 1S10 OD017992-01), and Novogene. The content is solely the responsibility of the authors and does not necessarily represent the official views of the National Institutes of Health.

AUTHOR CONTRIBUTIONS

Conceptualization, S.K., M.Z., and A.H.K.R.; investigation, S.K., M.Z., M.R.S., D.P., L.J., and R.E.M.; formal analysis, S.K., M.Z., D.P., and R.E.M.; visualization, S.K., M.R.S., and D.P.; methodology, S.A., B.V.L.V., and H.G.G.; resources, S.A., B.V.L.V., H.G.G., and J.O.B.; writing – original draft, S.K.; writing – review and editing, S.K., M.Z., B.V.L.V., H.G.G., S.-B.Q., J.O.B., and A.H.K.R.; supervision, H.G.G., S.-B.Q., J.O.B., and A.H.K.R.; project administration, A.H.K.R.; funding acquisition, H.G.G., J.O.B., and A.H.K.R.

DECLARATION OF INTERESTS

The authors declare no competing interests.

STAR★METHODS

Detailed methods are provided in the online version of this paper and include the following:

- KEY RESOURCES TABLE
- EXPERIMENTAL MODEL AND STUDY PARTICIPANT DETAILS
  - Plant material
  - Llama-tagged ARR7 construct
  - Plant growth conditions
- METHOD DETAILS
  - Flower staging
  - RNA-seq data collection and analysis
  - Proteomics
  - Polysome extraction and profiling
  - Puromycin labeling
  - TOR activity assay
  - Confocal microscopy
  - Visualization of tissue morphology
  - Quantification of sepal initiation robustness
  - Quantification of fluorescent reporters
  - *In vitro* drug treatments on inflorescence samples
  - *Torin2 and AZD-8055 treatment* in planta
  - Imaging of whole plant, whole inflorescence, silique, and mature sepals
  - Cytokinin extraction and measurement
  - Image processing software
- QUANTIFICATION AND STATISTICAL ANALYSIS
  - Statistical tests
  - Statistical software

SUPPLEMENTAL INFORMATION

Supplemental information can be found online at https://doi.org/10.1016/j.devcel.2024.08.010.

Received: May 12, 2023
Revised: April 15, 2024
Accepted: August 30, 2024
Published: September 20, 2024

REFERENCES

1. Kaneko, K. (2007). Evolution of robustness to noise and mutation in gene expression dynamics. PLoS One *2*, e434. https://doi.org/10.1371/journal.pone.0000434.
2. Lachowiec, J., Queitsch, C., and Kliebenstein, D.J. (2016). Molecular mechanisms governing differential robustness of development and environmental responses in plants. Ann. Bot. *117*, 795–809. https://doi.org/10.1093/aob/mcv151.
3. Zabinsky, R.A., Mason, G.A., Queitsch, C., and Jarosz, D.F. (2019). It's not magic – Hsp90 and its effects on genetic and epigenetic variation. Semin. Cell Dev. Biol. *88*, 21–35. https://doi.org/10.1016/j.semcdb.2018.05.015.
4. Waddington, C.H. (1942). Canalization of development and the inheritance of acquired characters. Nature *150*, 563–565.
5. Parker, J., and Struhl, G. (2020). Control of *Drosophila* wing size by morphogen range and hormonal gating. Proc. Natl. Acad. Sci. USA *117*, 31935–31944. https://doi.org/10.1073/pnas.2018196117.
6. Garelli, A., Gontijo, A.M., Miguela, V., Caparros, E., and Dominguez, M. (2012). Imaginal discs secrete insulin-like peptide 8 to mediate plasticity of growth and maturation. Science *336*, 579–582. https://doi.org/10.1126/science.1216735.
7. Crickmore, M.A., and Mann, R.S. (2006). Hox control of organ size by regulation of morphogen production and mobility. Science *313*, 63–68. https://doi.org/10.1126/science.1128650.
8. Recasens-Alvarez, C., Ferreira, A., and Milán, M. (2017). JAK/STAT controls organ size and fate specification by regulating morphogen production and signalling. Nat. Commun. *8*, 13815. https://doi.org/10.1038/ncomms13815.
9. King, S., Beck, F., and Lüttge, U. (2004). On the mystery of the golden angle in phyllotaxis. Plant Cell Environ. *27*, 685–695. https://doi.org/10.1111/j.1365-3040.2004.01185.x.
10. Smith, R.S., Guyomarc'h, S., Mandel, T., Reinhardt, D., Kuhlemeier, C., and Prusinkiewicz, P. (2006). A plausible model of phyllotaxis. Proc. Natl. Acad. Sci. USA *103*, 1301–1306. https://doi.org/10.1073/pnas.0510457103.
11. Besnard, F., Refahi, Y., Morin, V., Marteaux, B., Brunoud, G., Chambrier, P., Rozier, F., Mirabet, V., Legrand, J., Lainé, S., et al. (2014). Cytokinin signalling inhibitory fields provide robustness to phyllotaxis. Nature *505*, 417–421. https://doi.org/10.1038/nature12791.
12. Queitsch, C., Sangster, T.A., and Lindquist, S. (2002). Hsp90 as a capacitor of phenotypic variation. Nature *417*, 618–624. https://doi.org/10.1038/nature749.
13. Rutherford, S.L., and Lindquist, S. (1998). Hsp90 as a capacitor for morphological evolution. Nature *396*, 336–342. https://doi.org/10.1038/24550.
14. Lehner, B., Crombie, C., Tischler, J., Fortunato, A., and Fraser, A.G. (2006). Systematic mapping of genetic interactions in *Caenorhabditis elegans* identifies common modifiers of diverse signaling pathways. Nat. Genet. *38*, 896–903. https://doi.org/10.1038/ng1844.
15. Levy, S.F., and Siegal, M.L. (2008). Network hubs buffer environmental variation in *Saccharomyces cerevisiae*. PLoS Biol. *6*, e264. https://doi.org/10.1371/journal.pbio.0060264.
16. Folta, A., Severing, E.I., Krauskopf, J., van de Geest, H., Verver, J., Nap, J.P., and Mlynarova, L. (2014). Over-expression of Arabidopsis AtCHR23 chromatin remodeling ATPase results in increased variability of growth and gene expression. BMC Plant Biol. *14*, 76. https://doi.org/10.1186/1471-2229-14-76.
17. Hintze, M., Katsanos, D., Shahrezaei, V., and Barkoulas, M. (2021). Phenotypic robustness of epidermal stem cell number in *C. elegans* is modulated by the activity of the conserved N-acetyltransferase nath-10/NAT10. Front. Cell Dev. Biol. *9*, 640856. https://doi.org/10.3389/fcell.2021.640856.
18. Marygold, S.J., Roote, J., Reuter, G., Lambertsson, A., Ashburner, M., Millburn, G.H., Harrison, P.M., Yu, Z., Kenmochi, N., Kaufman, T.C., et al. (2007). The ribosomal protein genes and Minute loci of *Drosophila melanogaster*. Genome Biol. *8*, R216. https://doi.org/10.1186/gb-2007-8-10-r216.
19. Wang, S., Kurepa, J., and Smalle, J.A. (2009). The *Arabidopsis* 26S proteasome subunit RPN1a is required for optimal plant growth and stress responses. Plant Cell Physiol. *50*, 1721–1725. https://doi.org/10.1093/pcp/pcp105.
20. Gallois, J.L., Guyon-Debast, A., Lécureuil, A., Vezon, D., Carpentier, V., Bonhomme, S., and Guerche, P. (2009). The *Arabidopsis* proteasome RPT5 subunits are essential for gametophyte development and show accession-dependent redundancy. Plant Cell *21*, 442–459. https://doi.org/10.1105/tpc.108.062372.
21. Hong, L., DuMond, M., Tsugawa, S., Sapala, A., Routier-Kierzkowska, A.L., Zhou, Y., Chen, C., Kiss, A., Zhu, M., Hamant, O., et al. (2016). Variable cell growth yields reproducible organ development through spatiotemporal averaging. Dev. Cell *38*, 15–32. https://doi.org/10.1016/j.devcel.2016.06.016.
22. Roeder, A.H.K. (2021). Arabidopsis sepals: A model system for the emergent process of morphogenesis. Quant. Plant Biol. *2*, e14. https://doi.org/10.1017/qpb.2021.12.
23. Zhu, M., Chen, W., Mirabet, V., Hong, L., Bovio, S., Strauss, S., Schwarz, E.M., Tsugawa, S., Wang, Z., Smith, R.S., et al. (2020). Robust organ size requires robust timing of initiation orchestrated by focused auxin and cytokinin signalling. Nat. Plants *6*, 686–698. https://doi.org/10.1038/s41477-020-0666-7.

24. Kong, S., Zhu, M., and Roeder, A.H.K. (2024). Self-organization underlies developmental robustness in plants. Cells Dev. 203936. https://doi.org/10.1016/j.cdev.2024.203936.
25. Kong, S., Zhu, M., Pan, D., Lane, B., Smith, R.S., and Roeder, A.H.K. (2024). Tradeoff between speed and robustness in primordium initiation mediated by auxin-CUC1 interaction. Nat. Commun. *15*, 5911. https://doi.org/10.1038/s41467-024-50172-9.
26. Trinh, D.-C., Martin, M., Bald, L., Maizel, A., Trehin, C., and Hamant, O. (2023). Increased gene expression variability hinders the formation of regional mechanical conflicts leading to reduced organ shape robustness. Proc. Natl. Acad. Sci. USA *120*, e2302441120. https://doi.org/10.1073/pnas.2302441120.
27. Jing, H., and Strader, L.C. (2019). Interplay of auxin and cytokinin in lateral root development. Int. J. Mol. Sci. *20*, 486. https://doi.org/10.3390/ijms20030486.
28. Hussain, S., Nanda, S., Zhang, J., Rehmani, M.I.A., Suleman, M., Li, G., and Hou, H. (2021). Auxin and cytokinin interplay during leaf morphogenesis and phyllotaxy. Plants (Basel) *10*, 1732. https://doi.org/10.3390/plants10081732.
29. Schaller, G.E., Bishopp, A., and Kieber, J.J. (2015). The yin-yang of hormones: cytokinin and auxin interactions in plant development. Plant Cell *27*, 44–63. https://doi.org/10.1105/tpc.114.133595.
30. Ingargiola, C., Turqueto Duarte, G.T., Robaglia, C., Leprince, A.S., and Meyer, C. (2020). The plant target of rapamycin: A conduc TOR of nutrition and metabolism in photosynthetic organisms. Genes (Basel) *11*, 1285. https://doi.org/10.3390/genes11111285.
31. Scarpin, M.R., Leiboff, S., and Brunkard, J.O. (2020). Parallel global profiling of plant tor dynamics reveals a conserved role for LARP1 in translation. eLife *9*, e58795. https://doi.org/10.7554/eLife.58795.
32. Yu, H., Ito, T., Wellmer, F., and Meyerowitz, E.M. (2004). Repression of AGAMOUS-LIKE 24 is a crucial step in promoting flower development. Nat. Genet. *36*, 157–161. https://doi.org/10.1038/ng1286.
33. Wellmer, F., Alves-Ferreira, M., Dubois, A., Riechmann, J.L., and Meyerowitz, E.M. (2006). Genome-wide analysis of gene expression during early *Arabidopsis* flower development. PLoS Genet. *2*, 1012–1024. https://doi.org/10.1371/journal.pgen.0020117.
34. Smyth, D.R., Bowman, J.L., and Meyerowitz, E.M. (1990). Early flower development in Arabidopsis. Plant Cell *2*, 755–767. https://doi.org/10.1105/tpc.2.8.755.
35. Goodman, C.A., and Hornberger, T.A. (2013). Measuring protein synthesis with SUnSET: A valid alternative to traditional techniques? Exerc. Sport Sci. Rev. *41*, 107–115. https://doi.org/10.1097/JES.0b013e3182798a95.
36. Van Hoewyk, D. (2016). Use of the non-radioactive SUnSET method to detect decreased protein synthesis in proteasome inhibited Arabidopsis roots. Plant Methods *12*, 20. https://doi.org/10.1186/S13007-016-0120-Z.
37. Scarpin, M.R., Busche, M., Martinez, R.E., Harper, L.C., Reiser, L., Szakonyi, D., Merchante, C., Lan, T., Xiong, W., Mo, B., et al. (2023). An updated nomenclature for plant ribosomal protein genes. Plant Cell *35*, 640–643. https://doi.org/10.1093/plcell/koac333.
38. Brunkard, J.O. (2020). Exaptive evolution of target of rapamycin signaling in multicellular eukaryotes. Dev. Cell *54*, 142–155. https://doi.org/10.1016/j.devcel.2020.06.022.
39. Battaglioni, S., Benjamin, D., Wälchli, M., Maier, T., and Hall, M.N. (2022). mTOR substrate phosphorylation in growth control. Cell *185*, 1814–1836. https://doi.org/10.1016/j.cell.2022.04.013.
40. Valvezan, A.J., and Manning, B.D. (2019). Molecular logic of mTORC1 signalling as a metabolic rheostat. Nat. Metab. *1*, 321–333. https://doi.org/10.1038/s42255-019-0038-7.
41. Schepetilnikov, M., and Ryabova, L.A. (2018). Recent discoveries on the role of tor (Target of rapamycin) signaling in translation in plants. Plant Physiol. *176*, 1095–1105. https://doi.org/10.1104/pp.17.01243.
42. Scarpin, M.R., Simmons, C.H., and Brunkard, J.O. (2022). Translating across kingdoms: target of rapamycin promotes protein synthesis through conserved and divergent pathways in plants. J. Exp. Bot. *73*, 7016–7025. https://doi.org/10.1093/jxb/erac267.
43. Schepetilnikov, M., Kobayashi, K., Geldreich, A., Caranta, C., Robaglia, C., Keller, M., and Ryabova, L.A. (2011). Viral factor TAV recruits TOR/S6K1 signalling to activate reinitiation after long ORF translation. EMBO J. *30*, 1343–1356. https://doi.org/10.1038/emboj.2011.39.
44. Schepetilnikov, M., Dimitrova, M., Mancera-Martínez, E., Geldreich, A., Keller, M., and Ryabova, L.A. (2013). TOR and S6K1 promote translation reinitiation of uORF-containing mRNAs via phosphorylation of eIF3h. EMBO J. *32*, 1087–1102. https://doi.org/10.1038/emboj.2013.61.
45. Schepetilnikov, M., Makarian, J., Srour, O., Geldreich, A., Yang, Z., Chicher, J., Hammann, P., and Ryabova, L.A. (2017). GTPase ROP2 binds and promotes activation of target of rapamycin, TOR, in response to auxin. EMBO J. *36*, 886–903. https://doi.org/10.15252/embj.201694816.
46. Chen, G.H., Liu, M.J., Xiong, Y., Sheen, J., and Wu, S.H. (2018). TOR and RPS6 transmit light signals to enhance protein translation in deetiolating Arabidopsis seedlings. Proc. Natl. Acad. Sci. USA *115*, 12823–12828. https://doi.org/10.1073/pnas.1809526115.
47. Mancera-Martínez, E., Dong, Y., Makarian, J., Srour, O., Thiébeauld, O., Jamsheer, M., Chicher, J., Hammann, P., Schepetilnikov, M., and Ryabova, L.A. (2021). Phosphorylation of a reinitiation supporting protein, RISP, determines its function in translation reinitiation. Nucleic Acids Res. *49*, 6908–6924. https://doi.org/10.1093/nar/gkab501.
48. Dong, Y., Srour, O., Lukhovitskaya, N., Makarian, J., Baumberger, N., Galzitskaya, O., Elser, D., Schepetilnikov, M., and Ryabova, L.A. (2023). Functional analogs of mammalian 4E-BPs reveal a role for TOR in global plant translation. Cell Rep. *42*, 112892. https://doi.org/10.1016/j.celrep.2023.112892.
49. Dasgupta, A., Urquidi Camacho, R.A.U., Enganti, R., Cho, S.K., Tucker, L.L., Torreverde, J.S., Abraham, P.E., and von Arnim, A.G. (2024). A phosphorylation-deficient ribosomal protein eS6 is largely functional in Arabidopsis thaliana, rescuing mutant defects from global translation and gene expression to photosynthesis and growth. Plant Direct *8*, e566. https://doi.org/10.1002/pld3.566.
50. Xiong, Y., McCormack, M., Li, L., Hall, Q., Xiang, C., and Sheen, J. (2013). Glucose-TOR signalling reprograms the transcriptome and activates meristems. Nature *496*, 181–186. https://doi.org/10.1038/nature12030.
51. Riegler, S., Servi, L., Scarpin, M.R., Godoy Herz, M.A., Kubaczka, M.G., Venhuizen, P., Meyer, C., Brunkard, J.O., Kalyna, M., Barta, A., et al. (2021). Light regulates alternative splicing outcomes via the TOR kinase pathway. Cell Rep. *36*, 109676. https://doi.org/10.1016/j.celrep.2021.109676.
52. Obomighie, I., Lapenas, K., Murphy, B.E., Bowles, A.M.C., Bechtold, U., and Prischi, F. (2021). The role of ribosomal protein S6 kinases in plant homeostasis. Front. Mol. Biosci. *8*, 636560. https://doi.org/10.3389/fmolb.2021.636560.
53. Xiong, Y., and Sheen, J. (2012). Rapamycin and glucose-target of rapamycin (TOR) protein signaling in plants. J. Biol. Chem. *287*, 2836–2842. https://doi.org/10.1074/jbc.M111.300749.
54. Moreau, M., Azzopardi, M., Clément, G., Dobrenel, T., Marchive, C., Renne, C., Martin-Magniette, M.L., Taconnat, L., Renou, J.P., Robaglia, C., et al. (2012). Mutations in the *Arabidopsis* homolog of LST8/GβL, a partner of the target of rapamycin kinase, impair plant growth, flowering, and metabolic adaptation to long days. Plant Cell *24*, 463–481. https://doi.org/10.1105/tpc.111.091306.
55. Brunkard, J.O., Xu, M., Scarpin, M.R., Chatterjee, S., Shemyakina, E.A., Goodman, H.M., and Zambryski, P. (2020). TOR dynamically regulates plant cell-cell transport. Proc. Natl. Acad. Sci. USA *117*, 5049–5058. https://doi.org/10.1073/pnas.1919196117.
56. Menand, B., Desnos, T., Nussaume, L., Berger, F., Bouchez, D., Meyer, C., and Robaglia, C. (2002). Expression and disruption of the *Arabidopsis*

TOR (target of rapamycin) gene. Proc. Natl. Acad. Sci. USA *99*, 6422–6427. https://doi.org/10.1073/pnas.092141899.

57. Zhao, Z., Andersen, S.U., Ljung, K., Dolezal, K., Miotk, A., Schultheiss, S.J., and Lohmann, J.U. (2010). Hormonal control of the shoot stem-cell niche. Nature *465*, 1089–1092. https://doi.org/10.1038/nature09126.
58. Yoshida, S., Mandel, T., and Kuhlemeier, C. (2011). Stem cell activation by light guides plant organogenesis. Genes Dev. *25*, 1439–1450. https://doi.org/10.1101/gad.631211.
59. Nishimura, T., Wada, T., Yamamoto, K.T., and Okada, K. (2005). The *Arabidopsis* STV1 protein, responsible for translation reinitiation, is required for auxin-mediated gynoecium patterning. Plant Cell *17*, 2940–2953. https://doi.org/10.1105/tpc.105.036533.
60. Zhou, F., Roy, B., and von Arnim, A.G. (2010). Translation reinitiation and development are compromised in similar ways by mutations in translation initiation factor eIF3h and the ribosomal protein RPL24. BMC Plant Biol. *10*, 193. https://doi.org/10.1186/1471-2229-10-193.
61. Rosado, A., Li, R., Van De Ven, W., Hsu, E., and Raikhel, N.V. (2012). *Arabidopsis* ribosomal proteins control developmental programs through translational regulation of auxin response factors. Proc. Natl. Acad. Sci. USA *109*, 19537–19544. https://doi.org/10.1073/pnas.1214774109.
62. Cancé, C., Martin-Arevalillo, R., Boubekeur, K., and Dumas, R. (2022). Auxin response factors are keys to the many auxin doors. New Phytol. *235*, 402–419. https://doi.org/10.1111/nph.18159.
63. Kim, B.H., Cai, X., Vaughn, J.N., and Von Arnim, A.G. (2007). On the functions of the h subunit of eukaryotic initiation factor 3 in late stages of translation initiation. Genome Biol. *8*, R60. https://doi.org/10.1186/gb-2007-8-4-r60.
64. Von Arnim, A.G., Jia, Q., and Vaughn, J.N. (2014). Regulation of plant translation by upstream open reading frames. Plant Sci. *214*, 1–12. https://doi.org/10.1016/j.plantsci.2013.09.006.
65. Jones, B., Gunnerås, S.A., Petersson, S.V., Tarkowski, P., Graham, N., May, S., Dolezal, K., Sandberg, G., and Ljung, K. (2010). Cytokinin regulation of auxin synthesis in Arabidopsis involves a homeostatic feedback loop regulated via auxin and cytokinin signal transduction. Plant Cell *22*, 2956–2969. https://doi.org/10.1105/tpc.110.074856.
66. Marhavý, P., Duclercq, J., Weller, B., Feraru, E., Bielach, A., Offringa, R., Friml, J., Schwechheimer, C., Murphy, A., and Benková, E. (2014). Cytokinin controls polarity of PIN1-dependent Auxin transport during lateral root organogenesis. Curr. Biol. *24*, 1031–1037. https://doi.org/10.1016/j.cub.2014.04.002.
67. Ruzicka, K., Šimášková, M., Duclercq, J., Petrášek, J., Zažímalová, E., Simon, S., Friml, J., Van Montagu, M.C.E., and Benková, E. (2009). Cytokinin regulates root meristem activity via modulation of the polar auxin transport. Proc. Natl. Acad. Sci. USA *106*, 4284–4289. https://doi.org/10.1073/pnas.0900060106.
68. Karunadasa, S.S., Kurepa, J., Shull, T.E., and Smalle, J.A. (2020). Cytokinin-induced protein synthesis suppresses growth and osmotic stress tolerance. New Phytol. *227*, 50–64. https://doi.org/10.1111/nph.16519.
69. Szweykowska, A., Gwoidi, E., and Spychala, M. (1980). The cytokinin control of protein synthesis in plants. In Metabolism and Molecular Activities of Cytokinins, J. Guern and C. Peaud-Lenoel, eds. (Springer-Verlag), pp. 212–217. https://doi.org/10.1007/978-3-642-68035-9.
70. Woźny, A., and Gwóźdź, E.A. (1980). The effect of cytokinin on the polyribosome formation in cucumber cotyledons. Biochem. Physiol. Pflanzen *175*, 476–480. https://doi.org/10.1016/s0015-3796(80)80032-1.
71. Klyachko, N.L., Yakovleva, L.A., Shakirova, F.M., and Kulaeva, O.N. (1982). Cell-free translation of polyribosomes from detached pumpkin cotyledons: effects of starvation and cytokinin. Biol. Plant. *24*, 374–380. https://doi.org/10.1007/BF02909106.
72. Short, K.C., Tepfer, D.A., and Fosket, D.E. (1974). Regulation of polyribosome formation and cell division in cultured soybean cells by cytokinin. J. Cell Sci. *15*, 75–87.
73. Brenner, W.G., and Schmülling, T. (2012). Transcript profiling of cytokinin action in *Arabidopsis* roots and shoots discovers largely similar but also organ-specific responses. BMC Plant Biol. *12*, 112. https://doi.org/10.1186/1471-2229-12-112.
74. Kiba, T., Naitou, T., Koizumi, N., Yamashino, T., Sakakibara, H., and Mizuno, T. (2005). Combinatorial microarray analysis revealing Arabidopsis genes implicated in cytokinin responses through the His→Asp phosphorelay circuitry. Plant Cell Physiol. *46*, 339–355. https://doi.org/10.1093/pcp/pci033.
75. Černý, M., Kuklová, A., Hoehenwarter, W., Fragner, L., Novák, O., Rotková, G., Jedelský, P.L., Žáková, K., Šmehilová, M., Strnad, M., et al. (2013). Proteome and metabolome profiling of cytokinin action in Arabidopsis identifying both distinct and similar responses to cytokinin down- and up-regulation. J. Exp. Bot. *64*, 4193–4206. https://doi.org/10.1093/jxb/ert227.
76. Cerný, M., Dycka, F., Bobál'Ová, J., and Brzobohatý, B. (2011). Early cytokinin response proteins and phosphoproteins of Arabidopsis thaliana identified by proteome and phosphoproteome profiling. J. Exp. Bot. *62*, 921–937. https://doi.org/10.1093/jxb/erq322.
77. Ren, B., Liang, Y., Deng, Y., Chen, Q., Zhang, J., Yang, X., and Zuo, J. (2009). Genome-wide comparative analysis of type-A Arabidopsis response regulator genes by overexpression studies reveals their diverse roles and regulatory mechanisms in cytokinin signaling. Cell Res. *19*, 1178–1190. https://doi.org/10.1038/cr.2009.88.
78. Ferreira, F.J., and Kieber, J.J. (2005). Cytokinin signaling. Curr. Opin. Plant Biol. *8*, 518–525. https://doi.org/10.1016/j.pbi.2005.07.013.
79. Kakimoto, T. (2003). Perception and signal transduction of cytokinins. Annu. Rev. Plant Biol. *54*, 605–627. https://doi.org/10.1146/annurev.arplant.54.031902.134802.
80. Jain, M., Tyagi, A.K., and Khurana, J.P. (2006). Molecular characterization and differential expression of cytokinin-responsive type-A response regulators in rice (*Oryza sativa*). BMC Plant Biol. *6*, 1. https://doi.org/10.1186/1471-2229-6-1.
81. To, J.P.C., Haberer, G., Ferreira, F.J., Deruère, J., Mason, M.G., Schaller, G.E., Alonso, J.M., Ecker, J.R., and Kieber, J.J. (2004). Type-A Arabidopsis response regulators are partially redundant negative regulators of cytokinin signaling. Plant Cell *16*, 658–671. https://doi.org/10.1105/tpc.018978.
82. Kiba, T., Yamada, H., Sato, S., Kato, T., Tabata, S., Yamashino, T., and Mizuno, T. (2003). The type-A response regulator, ARR15, acts as a negative regulator in the cytokinin-mediated signal transduction in *Arabidopsis thaliana*. Plant Cell Physiol. *44*, 868–874. https://doi.org/10.1093/pcp/pcg108.
83. Bothma, J.P., Norstad, M.R., Alamos, S., and Garcia, H.G. (2018). LlamaTags: A versatile tool to image transcription factor dynamics in live embryos. Cell *173*, 1810–1822.e16. https://doi.org/10.1016/j.cell.2018.03.069.
84. Acheampong, A.K., Shanks, C., Cheng, C.Y., Schaller, G.E., Dagdas, Y., and Kieber, J.J. (2020). EXO70D isoforms mediate selective autophagic degradation of type-A ARR proteins to regulate cytokinin sensitivity. Proc. Natl. Acad. Sci. USA *117*, 27034–27043. https://doi.org/10.1073/pnas.2013161117.
85. To, J.P.C., Deruère, J., Maxwell, B.B., Morris, V.F., Hutchison, C.E., Ferreira, F.J., Schaller, G.E., and Kieber, J.J. (2007). Cytokinin regulates type-A Arabidopsis response regulator activity and protein stability via two-component phosphorelay. Plant Cell *19*, 3901–3914. https://doi.org/10.1105/tpc.107.052662.
86. Imamura, A., Yoshino, Y., and Mizuno, T. (2001). Cellular localization of the signaling components of Arabidopsis his-to-Asp phosphorelay. Biosci. Biotechnol. Biochem. *65*, 2113–2117. https://doi.org/10.1271/bbb.65.2113.
87. Lee, D.J., Kim, S., Ha, Y.M., and Kim, J. (2008). Phosphorylation of Arabidopsis response regulator 7 (ARR7) at the putative phospho-accepting site is required for ARR7 to act as a negative regulator of

cytokinin signaling. Planta *227*, 577–587. https://doi.org/10.1007/s00425-007-0640-x.

88. Buechel, S., Leibfried, A., To, J.P.C., Zhao, Z., Andersen, S.U., Kieber, J.J., and Lohmann, J.U. (2010). Role of A-type Arabidopsis Response Regulators in meristem maintenance and regeneration. Eur. J. Cell Biol. *89*, 279–284. https://doi.org/10.1016/j.ejcb.2009.11.016.

89. Xie, M., Chen, H., Huang, L., O'Neil, R.C., Shokhirev, M.N., and Ecker, J.R. (2018). A B-ARR-mediated cytokinin transcriptional network directs hormone cross-regulation and shoot development. Nat. Commun. *9*, 1604. https://doi.org/10.1038/s41467-018-03921-6.

90. Mähönen, A.P., Bishopp, A., Higuchi, M., Nieminen, K.M., Kinoshita, K., Törmäkangas, K., Ikeda, Y., Oka, A., Kakimoto, T., and Helariutta, Y. (2006). Cytokinin signaling and its inhibitor AHP6 regulate cell fate during vascular development. Science *311*, 94–98. https://doi.org/10.1126/science.1118875.

91. Kieber, J.J., and Schaller, G.E. (2018). Cytokinin signaling in plant development. Development *145*, dev149344. https://doi.org/10.1242/dev.149344.

92. Hwang, I., Chen, H.C., and Sheen, J. (2002). Two-component signal transduction pathways in Arabidopsis. Plant Physiol. *129*, 500–515. https://doi.org/10.1104/pp.005504.

93. Feng, J., Wang, C., Chen, Q., Chen, H., Ren, B., Li, X., and Zuo, J. (2013). S-nitrosylation of phosphotransfer proteins represses cytokinin signaling. Nat. Commun. *4*, 1529. https://doi.org/10.1038/ncomms2541.

94. Zhang, W., To, J.P.C., Cheng, C.Y., Schaller, G.E., and Kieber, J.J. (2011). Type-A response regulators are required for proper root apical meristem function through post-transcriptional regulation of PIN auxin efflux carriers. Plant J. *68*, 1–10. https://doi.org/10.1111/j.1365-313X.2011.04668.x.

95. Abel, S., Nguyen, M.D., and Theologis, A. (1995). The *PS-IAA4/5-like* family of early auxin-inducible mRNAs in *Arabidopsis thaliana*. J. Mol. Biol. *251*, 533–549. https://doi.org/10.1006/jmbi.1995.0454.

96. Park, J.Y., Kim, H.J., and Kim, J. (2002). Mutation in domain II of IAA1 confers diverse auxin-related phenotypes and represses auxin-activated expression of Aux/IAA genes in steroid regulator-inducible system. Plant J. *32*, 669–683. https://doi.org/10.1046/j.1365-313X.2002.01459.x.

97. Abel, S., Oeller, P.W., and Theologis, A. (1994). Early auxin-induced genes encode short-lived nuclear proteins. Proc. Natl. Acad. Sci. USA *91*, 326–330. https://doi.org/10.1073/pnas.91.1.326.

98. Zenser, N., Ellsmore, A., Leasure, C., and Callis, J. (2001). Auxin modulates the degradation rate of Aux/IAA proteins. Proc. Natl. Acad. Sci. USA *98*, 11795–11800. https://doi.org/10.1073/pnas.211312798.

99. Worley, C.K., Zenser, N., Ramos, J., Rouse, D., Leyser, O., Theologis, A., and Callis, J. (2000). Degradation of Aux/IAA proteins is essential for normal auxin signalling. Plant J. *21*, 553–562. https://doi.org/10.1046/j.1365-313X.2000.00703.x.

100. Ramos, J.A., Zenser, N., Leyser, O., and Callis, J. (2001). Rapid degradation of auxin/indoleacetic acid proteins requires conserved amino acids of domain II and is proteasome dependent. Plant Cell *13*, 2349–2360. https://doi.org/10.1105/tpc.13.10.2349.

101. de Figueiredo, M.R.A., and Strader, L.C. (2022). Intrinsic and extrinsic regulators of Aux/IAA protein degradation dynamics. Trends Biochem. Sci. *47*, 865–874. https://doi.org/10.1016/j.tibs.2022.06.004.

102. Liao, C.Y., Smet, W., Brunoud, G., Yoshida, S., Vernoux, T., and Weijers, D. (2015). Reporters for sensitive and quantitative measurement of auxin response. Nat. Methods *12*, 207–210. https://doi.org/10.1038/nmeth.3279.

103. Mills, E.W., and Green, R. (2017). Ribosomopathies: there's strength in numbers. Science *358*, eaan2755. https://doi.org/10.1126/science.aan2755.

104. Warren, A.J. (2018). Molecular basis of the human ribosomopathy Shwachman-Diamond syndrome. Adv. Biol. Regul. *67*, 109–127. https://doi.org/10.1016/j.jbior.2017.09.002.

105. Hawer, H., Mendelsohn, B.A., Mayer, K., Kung, A., Malhotra, A., Tuupanen, S., Schleit, J., Brinkmann, U., and Schaffrath, R. (2020). Diphthamide-deficiency syndrome: a novel human developmental disorder and ribosomopathy. Eur. J. Hum. Genet. *28*, 1497–1508. https://doi.org/10.1038/s41431-020-0668-y.

106. Armistead, J., Patel, N., Wu, X., Hemming, R., Chowdhury, B., Basra, G.S., Del Bigio, M.R., Ding, H., and Triggs-Raine, B. (2015). Growth arrest in the ribosomopathy, bowen-conradi syndrome, is due to dramatically reduced cell proliferation and a defect in mitotic progression. Biochim. Biophys. Acta *1852*, 1029–1037. https://doi.org/10.1016/j.bbadis.2015.02.007.

107. Zhou, C., Zang, D., Jin, Y., Wu, H., Liu, Z., Du, J., and Zhang, J. (2011). Mutation in ribosomal protein L21 underlies hereditary hypotrichosis simplex. Hum. Mutat. *32*, 710–714. https://doi.org/10.1002/humu.21503.

108. Dixon, M.J. (1995). Treacher Collins syndrome. J. Med. Genet. *32*, 806–808. https://doi.org/10.1136/jmg.32.10.806.

109. Gazda, H.T., Sheen, M.R., Vlachos, A., Choesmel, V., O'Donohue, M.F., Schneider, H., Darras, N., Hasman, C., Sieff, C.A., Newburger, P.E., et al. (2008). Ribosomal protein L5 and L11 mutations are associated with cleft palate and abnormal thumbs in Diamond-Blackfan anemia patients. Am. J. Hum. Genet. *83*, 769–780. https://doi.org/10.1016/j.ajhg.2008.11.004.

110. Oliver, E.R., Saunders, T.L., Tarlé, S.A., and Glaser, T. (2004). Ribosomal protein L24 defect in belly spot and tail (*Bst*), a mouse *Minute*. Development *131*, 3907–3920. https://doi.org/10.1242/dev.01268.

111. McGowan, K.A., Li, J.Z., Park, C.Y., Beaudry, V., Tabor, H.K., Sabnis, A.J., Zhang, W., Fuchs, H., De Angelis, M.H., Myers, R.M., et al. (2008). Ribosomal mutations cause p53-mediated dark skin and pleiotropic effects. Nat. Genet. *40*, 963–970. https://doi.org/10.1038/ng.188.

112. Oristian, D.S., Sloofman, L.G., Zhou, X., Wang, L., Farach-Carson, M.C., and Kirn-Safran, C.B. (2009). Ribosomal protein L29/HIP deficiency delays osteogenesis and increases fragility of adult bone in mice. J. Orthop. Res. *27*, 28–35. https://doi.org/10.1002/jor.20706.

113. Uechi, T., Nakajima, Y., Nakao, A., Torihara, H., Chakraborty, A., Inoue, K., and Kenmochi, N. (2006). Ribosomal protein gene knockdown causes developmental defects in zebrafish. PLoS One *1*, e37. https://doi.org/10.1371/journal.pone.0000037.

114. Marygold, S.J., Coelho, C.M.A., and Leevers, S.J. (2005). Genetic analysis of RpL38 and RpL5, two minute genes located in the centric heterochromatin of chromosome 2 of *Drosophila melanogaster*. Genetics *169*, 683–695. https://doi.org/10.1534/genetics.104.034124.

115. Lee, C.C., Tsai, Y.T., Kao, C.W., Lee, L.W., Lai, H.J., Ma, T.H., Chang, Y.S., Yeh, N.H., and Lo, S.J. (2014). Mutation of a Nopp140 gene *dao-5* alters rDNA transcription and increases germ cell apoptosis in *C. elegans*. Cell Death Dis. *5*, e1158. https://doi.org/10.1038/cddis.2014.114.

116. Ito, T., Kim, G.T., and Shinozaki, K. (2000). Disruption of an Arabidopsis cytoplasmic ribosomal protein S13-homologous gene by transposon-mediated mutagenesis causes aberrant growth and development. Plant J. *22*, 257–264. https://doi.org/10.1046/j.1365-313X.2000.00728.x.

117. Horiguchi, G., Mollá-Morales, A., Pérez-Pérez, J.M., Kojima, K., Robles, P., Ponce, M.R., Micol, J.L., and Tsukaya, H. (2011). Differential contributions of ribosomal protein genes to *Arabidopsis thaliana* leaf development. Plant J. *65*, 724–736. https://doi.org/10.1111/j.1365-313X.2010.04457.x.

118. Zhao, H., Lü, S., Li, R., Chen, T., Zhang, H., Cui, P., Ding, F., Liu, P., Wang, G., Xia, Y., et al. (2015). The Arabidopsis gene *DIG6* encodes a large 60S subunit nuclear export GTPase 1 that is involved in ribosome biogenesis and affects multiple auxin-regulated development processes. J. Exp. Bot. *66*, 6863–6875. https://doi.org/10.1093/jxb/erv391.

119. Takagi, M., Absalon, M.J., McLure, K.G., and Kastan, M.B. (2005). Regulation of p53 translation and induction after DNA damage by ribosomal protein L26 and nucleolin. Cell *123*, 49–63. https://doi.org/10.1016/j.cell.2005.07.034.

120. Deisenroth, C., and Zhang, Y. (2010). Ribosome biogenesis surveillance: probing the ribosomal protein-Mdm2-p53 pathway. Oncogene *29*, 4253–4260. https://doi.org/10.1038/onc.2010.189.

121. Warner, J.R., and McIntosh, K.B. (2009). How common are extraribosomal functions of ribosomal proteins? Mol. Cell *34*, 3–11. https://doi.org/10.1016/j.molcel.2009.03.006.

122. Dutt, S., Narla, A., Lin, K., Mullally, A., Abayasekara, N., Megerdichian, C., Wilson, F.H., Currie, T., Khanna-Gupta, A., Berliner, N., et al. (2011). Haploinsufficiency for ribosomal protein genes causes selective activation of p53 in human erythroid progenitor cells. Blood *117*, 2567–2576. https://doi.org/10.1182/blood-2010-07-295238.

123. Danilova, N., Sakamoto, K.M., and Lin, S. (2008). Ribosomal protein S19 deficiency in zebrafish leads to developmental abnormalities and defective erythropoiesis through activation of p53 protein family. Blood *112*, 5228–5237. https://doi.org/10.1182/blood-2008-01-132290.

124. Girardi, T., Vereecke, S., Sulima, S.O., Khan, Y., Fancello, L., Briggs, J.W., Schwab, C., De Beeck, J.O., Verbeeck, J., Royaert, J., et al. (2018). The T-cell leukemia-associated ribosomal RPL10 R98S mutation enhances JAK-STAT signaling. Leukemia *32*, 809–819. https://doi.org/10.1038/leu.2017.225.

125. Ludwig, L.S., Gazda, H.T., Eng, J.C., Eichhorn, S.W., Thiru, P., Ghazvinian, R., George, T.I., Gotlib, J.R., Beggs, A.H., Sieff, C.A., et al. (2014). Altered translation of GATA1 in Diamond-Blackfan anemia. Nat. Med. *20*, 748–753. https://doi.org/10.1038/nm.3557.

126. Khajuria, R.K., Munschauer, M., Ulirsch, J.C., Fiorini, C., Ludwig, L.S., McFarland, S.K., Abdulhay, N.J., Specht, H., Keshishian, H., Mani, D.R., et al. (2018). Ribosome levels selectively regulate translation and lineage commitment in human hematopoiesis. Cell *173*, 90–103.e19. https://doi.org/10.1016/j.cell.2018.02.036.

127. In, K., Zaini, M.A., Müller, C., Warren, A.J., Von Lindern, M., and Calkhoven, C.F. (2016). Shwachman-Bodian-Diamond syndrome (SBDS) protein deficiency impairs translation re-initiation from C/EBPα and C/EBPβ mRNAs. Nucleic Acids Res. *44*, 4134–4146. https://doi.org/10.1093/nar/gkw005.

128. Kondrashov, N., Pusic, A., Stumpf, C.R., Shimizu, K., Hsieh, A.C., Ishijima, J., Shiroishi, T., and Barna, M. (2011). Ribosome-mediated specificity in Hox mRNA translation and vertebrate tissue patterning. Cell *145*, 383–397. https://doi.org/10.1016/j.cell.2011.03.028.

129. Deliu, L.P., Turingan, M., Jadir, D., Lee, B., Ghosh, A., and Grewal, S.S. (2022). Serotonergic neuron ribosomal proteins regulate the neuroendocrine control of Drosophila development. PLoS Genet. *18*, e1010371. https://doi.org/10.1371/journal.pgen.1010371.

130. Adams, K.W., and Cooper, G.M. (2007). Rapid turnover of Mcl-1 couples translation to cell survival and apoptosis. J. Biol. Chem. *282*, 6192–6200. https://doi.org/10.1074/jbc.M610643200.

131. D'Agostino, I.B., Deruère, J., and Kieber, J.J. (2000). Characterization of the response of the Arabidopsis response regulator gene family to cytokinin. Plant Physiol. *124*, 1706–1717. https://doi.org/10.1104/pp.124.4.1706.

132. Bishopp, A., Help, H., El-Showk, S., Weijers, D., Scheres, B., Friml, J., Benková, E., Mähönen, A.P., and Helariutta, Y. (2011). A mutually inhibitory interaction between auxin and cytokinin specifies vascular pattern in roots. Curr. Biol. *21*, 917–926. https://doi.org/10.1016/j.cub.2011.04.017.

133. Huo, H.H., Luo, M., Lee, Y.-R.J., and Liu, B. (2023). The Microspherule protein 1(MCRS1) homolog interacts with the Myb-like transcription factor DRMY1 and is essential for embryogenesis in Arabidopsis thaliana. Preprint at bioRxiv. https://doi.org/10.1101/2023.07.11.548616.

134. Fawal, M.A., Brandt, M., and Djouder, N. (2015). MCRS1 binds and couples rheb to amino acid-dependent mTORC1 activation. Dev. Cell *33*, 67–81. https://doi.org/10.1016/j.devcel.2015.02.010.

135. Radhakrishnan, S.K., Lee, C.S., Young, P., Beskow, A., Chan, J.Y., and Deshaies, R.J. (2010). Transcription factor Nrf1 mediates the proteasome recovery pathway after proteasome inhibition in mammalian cells. Mol. Cell *38*, 17–28. https://doi.org/10.1016/j.molcel.2010.02.029.

136. Gladman, N.P., Marshall, R.S., Lee, K.H., and Vierstra, R.D. (2016). The proteasome stress regulon is controlled by a pair of NAC transcription factors in Arabidopsis. Plant Cell *28*, 1279–1296. https://doi.org/10.1105/tpc.15.01022.

137. Njomen, E., and Tepe, J.J. (2019). Proteasome activation as a new therapeutic approach to target proteotoxic disorders. J. Med. Chem. *62*, 6469–6481. https://doi.org/10.1021/acs.jmedchem.9b00101.

138. Anderson, R.T., Bradley, T.A., and Smith, D.M. (2022). Hyperactivation of the proteasome in Caenorhabditis elegans protects against proteotoxic stress and extends lifespan. J. Biol. Chem. *298*, 102415. https://doi.org/10.1016/j.jbc.2022.102415.

139. Kandel, R., Jung, J., and Neal, S. (2024). Proteotoxic stress and the ubiquitin proteasome system. Semin. Cell Dev. Biol. *156*, 107–120. https://doi.org/10.1016/j.semcdb.2023.08.002.

140. Quy, P.N., Kuma, A., Pierre, P., and Mizushima, N. (2013). Proteasome-dependent activation of mammalian target of rapamycin complex 1 (mTORC1) is essential for autophagy suppression and muscle remodeling following denervation. J. Biol. Chem. *288*, 1125–1134. https://doi.org/10.1074/jbc.M112.399949.

141. Zhao, J., Zhai, B., Gygi, S.P., and Goldberg, A.L. (2015). MTOR inhibition activates overall protein degradation by the ubiquitin proteasome system as well as by autophagy. Proc. Natl. Acad. Sci. USA *112*, 15790–15797. https://doi.org/10.1073/pnas.1521919112.

142. Zhang, Y., Nicholatos, J., Dreier, J.R., Ricoult, S.J.H., Widenmaier, S.B., Hotamisligil, G.S., Kwiatkowski, D.J., and Manning, B.D. (2014). Coordinated regulation of protein synthesis and degradation by mTORC1. Nature *513*, 440–443. https://doi.org/10.1038/nature13492.

143. Zhao, J., Garcia, G.A., and Goldberg, A.L. (2016). Control of proteasomal proteolysis by mTOR. Nature *529*, E1–E2. https://doi.org/10.1038/nature16472.

144. Zhang, Y., and Manning, B.D. (2016). Zhang & Manning reply. Nature *529*, E2–E3. https://doi.org/10.1038/nature16473.

145. Rousseau, A., and Bertolotti, A. (2016). An evolutionarily conserved pathway controls proteasome homeostasis. Nature *536*, 184–189. https://doi.org/10.1038/nature18943.

146. Perez-Riverol, Y., Bai, J., Bandla, C., García-Seisdedos, D., Hewapathirana, S., Kamatchinathan, S., Kundu, D.J., Prakash, A., Frericks-Zipper, A., Eisenacher, M., et al. (2022). The PRIDE database resources in 2022: A hub for mass spectrometry-based proteomics evidences. Nucleic Acids Res. *50*, D543–D552. https://doi.org/10.1093/nar/gkab1038.

147. Sud, M., Fahy, E., Cotter, D., Azam, K., Vadivelu, I., Burant, C., Edison, A., Fiehn, O., Higashi, R., Nair, K.S., et al. (2016). Metabolomics Workbench: an international repository for metabolomics data and metadata, metabolite standards, protocols, tutorials and training, and analysis tools. Nucleic Acids Res. *44*, D463–D470. https://doi.org/10.1093/nar/gkv1042.

148. Mähönen, A.P., Bonke, M., Kauppinen, L., Riikonen, M., Benfey, P.N., and Helariutta, Y. (2000). A novel two-component hybrid molecule regulates vascular morphogenesis of the Arabidopsis root. Genes Dev. *14*, 2938–2943. https://doi.org/10.1101/gad.189200.

149. Sotta, N., Shantikumar, L., Sakamoto, T., Matsunaga, S., and Fujiwara, T. (2016). TPR5 is involved in directional cell division and is essential for the maintenance of meristem cell organization in *Arabidopsis thaliana*. J. Exp. Bot. *67*, 2401–2411. https://doi.org/10.1093/jxb/erw043.

150. Heisler, M.G., Ohno, C., Das, P., Sieber, P., Reddy, G.V., Long, J.A., and Meyerowitz, E.M. (2005). Patterns of auxin transport and gene expression during primordium development revealed by live imaging of the Arabidopsis inflorescence meristem. Curr. Biol. *15*, 1899–1911. https://doi.org/10.1016/j.cub.2005.09.052.

151. Müller, B., and Sheen, J. (2008). Cytokinin and auxin interaction in root stem-cell specification during early embryogenesis. Nature *453*, 1094–1097. https://doi.org/10.1038/nature06943.

152. Brackmann, K., Qi, J., Gebert, M., Jouannet, V., Schlamp, T., Grünwald, K., Wallner, E.S., Novikova, D.D., Levitsky, V.G., Agustí, J., et al. (2018). Spatial specificity of auxin responses coordinates wood formation. Nat. Commun. *9*, 875. https://doi.org/10.1038/s41467-018-03256-2.
153. Argyros, R.D., Mathews, D.E., Chiang, Y.H., Palmer, C.M., Thibault, D.M., Etheridge, N., Argyros, D.A., Mason, M.G., Kieber, J.J., and Schaller, G.E. (2008). Type B response regulators of Arabidopsis play key roles in cytokinin signaling and plant development. Plant Cell *20*, 2102–2116. https://doi.org/10.1105/tpc.108.059584.
154. Rademacher, E.H., Möller, B., Lokerse, A.S., Llavata-Peris, C.I., Van Den Berg, W., and Weijers, D. (2011). A cellular expression map of the *Arabidopsis AUXIN RESPONSE FACTOR* gene family. Plant J. *68*, 597–606. https://doi.org/10.1111/j.1365-313X.2011.04710.x.
155. Saerens, D., Pellis, M., Loris, R., Pardon, E., Dumoulin, M., Matagne, A., Wyns, L., Muyldermans, S., and Conrath, K. (2005). Identification of a universal VHH framework to graft non-canonical antigen-binding loops of camel single-domain antibodies. J. Mol. Biol. *352*, 597–607. https://doi.org/10.1016/j.jmb.2005.07.038.
156. Fujii, Y., and Kodama, Y. (2015). *In planta* comparative analysis of improved green fluorescent proteins with reference to fluorescence intensity and bimolecular fluorescence complementation ability. Plant Biotechnol. *32*, 81–87. https://doi.org/10.5511/plantbiotechnology.15.0120a.
157. Alamos, S., Reimer, A., Niyogi, K.K., and Garcia, H.G. (2021). Quantitative imaging of RNA polymerase II activity in plants reveals the single-cell basis of tissue-wide transcriptional dynamics. Nat. Plants *7*, 1037–1049. https://doi.org/10.1038/s41477-021-00976-0.
158. Bolger, A.M., Lohse, M., and Usadel, B. (2014). Trimmomatic: a flexible trimmer for Illumina sequence data. Bioinformatics *30*, 2114–2120. https://doi.org/10.1093/bioinformatics/btu170.
159. Patro, R., Duggal, G., Love, M.I., Irizarry, R.A., and Kingsford, C. (2017). Salmon provides fast and bias-aware quantification of transcript expression. Nat. Methods *14*, 417–419. https://doi.org/10.1038/nmeth.4197.
160. Love, M.I., Huber, W., and Anders, S. (2014). Moderated estimation of fold change and dispersion for RNA-seq data with DESeq2. Genome Biol. *15*, 550. https://doi.org/10.1186/s13059-014-0550-8.
161. Alexa, A., Rahnenführer, J., and Lengauer, T. (2006). Improved scoring of functional groups from gene expression data by decorrelating GO graph structure. Bioinformatics *22*, 1600–1607. https://doi.org/10.1093/bioinformatics/btl140.
162. Mustroph, A., Juntawong, P., and Bailey-Serres, J. (2009). Isolation of plant polysomal mRNA by differential centrifugation and ribosome immunopurification methods. In Methods in Molecular Biology, *553* (Humana Press, a part of Springer Science+Business Media, LLC), pp. 109–126. https://doi.org/10.1007/978-1-60327-563-7_6.
163. Gao, X., Wan, J., Liu, B., Ma, M., Shen, B., and Qian, S.B. (2015). Quantitative profiling of initiating ribosomes *in vivo*. Nat. Methods *12*, 147–153. https://doi.org/10.1038/nmeth.3208.
164. Busche, M., Scarpin, M.R., Hnasko, R., and Brunkard, J.O. (2021). TOR coordinates nucleotide availability with ribosome biogenesis in plants. Plant Cell *33*, 1615–1632. https://doi.org/10.1093/plcell/koab043.
165. Schindelin, J., Rueden, C.T., Hiner, M.C., and Eliceiri, K.W. (2015). The ImageJ ecosystem: an open platform for biomedical image analysis. Mol. Reprod. Dev. *82*, 518–529. https://doi.org/10.1002/mrd.22489.
166. Schindelin, J., Arganda-Carreras, I., Frise, E., Kaynig, V., Longair, M., Pietzsch, T., Preibisch, S., Rueden, C., Saalfeld, S., Schmid, B., et al. (2012). Fiji: an open-source platform for biological-image analysis. Nat. Methods *9*, 676–682. https://doi.org/10.1038/nmeth.2019.
167. Barbier de Reuille, P.B., Routier-Kierzkowska, A.L., Kierzkowski, D., Bassel, G.W., Schüpbach, T., Tauriello, G., Bajpai, N., Strauss, S., Weber, A., Kiss, A., et al. (2015). MorphoGraphX: A platform for quantifying morphogenesis in 4D. eLife *4*, 05864. https://doi.org/10.7554/eLife.05864.
168. Schäfer, M., Brütting, C., Baldwin, I.T., and Kallenbach, M. (2016). High-throughput quantification of more than 100 primary- and secondary-metabolites, and phytohormones by a single solid-phase extraction based sample preparation with analysis by UHPLC-HESI-MS/MS. Plant Methods *12*, 30. https://doi.org/10.1186/s13007-016-0130-x.
169. Kojima, M., Kamada-Nobusada, T., Komatsu, H., Takei, K., Kuroha, T., Mizutani, M., Ashikari, M., Ueguchi-Tanaka, M., Matsuoka, M., Suzuki, K., et al. (2009). Highly sensitive and high-throughput analysis of plant hormones using ms-probe modification and liquid chromatographytandem mass spectrometry: an application for hormone profiling in Oryza sativa. Plant Cell Physiol. *50*, 1201–1214. https://doi.org/10.1093/pcp/pcp057.
170. Novák, O., Antoniadi, I., and Ljung, K. (2017). High-resolution cell-type specific analysis of cytokinins in sorted root cell populations of *Arabidopsis thaliana*. Methods Mol. Biol. *1497*, 231–248. https://doi.org/10.1007/978-1-4939-6469-7_1.
171. R Core Team (2021). R: A Language and Environment for Statistical Computing (R Foundation for Statistical Computing). https://www.R-project.org/.
172. Wickham, H. (2009). ggplot2: Elegant Graphics for Data Analysis, R. Gentleman, K. Hornik, and G. Parmigiani, eds. (Springer). https://doi.org/10.1007/978-0-387-98141-3.

Please cite this article in press as: Kong et al., DRMY1 promotes robust morphogenesis in *Arabidopsis* by sustaining the translation of cytokinin-signaling inhibitor proteins, Developmental Cell (2024), https://doi.org/10.1016/j.devcel.2024.08.010

STAR★METHODS

KEY RESOURCES TABLE

REAGENT or RESOURCE	SOURCE	IDENTIFIER
Antibodies		
Mouse-origin anti-puromycin monoclonal antibody	Millipore Sigma	Cat# MABE343; RRID: AB_2566826
Goat-anti-mouse HRP-conjugated secondary antibody	Abcam	Cat# ab6789; RRID: AB_955439
Deposited data		
RNA-seq data for *ap1 cal AP1-GR* and *drmy1 ap1 cal AP1-GR* inflorescence tissue	This study	NCBI GEO: GSE230100
RNA-seq data for WT and *drmy1* seedlings treated with mock or AZD-8055	This study	NIH BioProject: PRJNA961813
Mass spectrometry data for proteomics	This study	ProteomeXchange Consortium via the PRIDE partner repository: PXD041723
Mass spectrometry data for cytokinins	This study	NIH National Metabolomics Data Repository (NMDR) website, the Metabolomics Workbench: ST002571
Experimental models: Organisms/strains		
Arabidopsis: Col-0: WT	N/A	RRID:NCBITaxon_3702
Arabidopsis: *wol*: *wol-1*	Mähönen et al.[148]	N/A
Arabidopsis: *spaghetti-1*: *tpr5-1*	Sotta et al.[149]	N/A
Arabidopsis: *ahp6*: *ahp6*	Besnard et al.[11]	N/A
Arabidopsis: *arr3,4,5,6,7,8,9,15*: *arr3,4,5,6,7,8,9,15*	Zhang et al.[94]	N/A
Arabidopsis: *ap1 cal AP1-GR*: *ap1 cal 35S::AP1-GR*	Yu et al.[32] and Wellmer et al.[33]	N/A
Arabidopsis: *arr1 35S::ARR1*: *arr1-1 35S::ARR1*	Karunadasa et al.[68]	N/A
Arabidopsis: DR5: *DR5::3xVENUS-N7*	Heisler et al.[150]	N/A
Arabidopsis: TCS: *TCS::GFP*	Müller et al.[151]	N/A
Arabidopsis: *pARF5::erYFP*: *pARF5::ER-EYFP-HDEL*	Brackmann et al.[152]	N/A
Arabidopsis: R2D2: *pUS7Y-mDII-NtdTomato-pUS7Y-DII-N3xVENUS*	Liao et al.[102]	N/A
Arabidopsis: *35S::mCirtine-RCI2A*: *35S::mCirtine-RCI2A*	Zhu et al.[23]	N/A
Arabidopsis: *UBQ10::mCherry-RCI2A*: *UBQ10::mCherry-RCI2A*	Zhu et al.[23]	N/A
Arabidopsis: *pAHP3::AHP3-GFP*: *pAHP3::AHP3-GFP*	Feng et al.[93]	N/A
Arabidopsis: *pAHP6::AHP6-VENUS*: *pAHP6::AHP6-VENUS*	Besnard et al.[11]	N/A
Arabidopsis: *pAHP6::GFP-ER*: *pAHP6::GFP-ER*	Besnard et al.[11] and Mähönen et al.[90]	N/A
Arabidopsis: *ul4z*: *ul4z*	Arabidopsis Biological Resource Center (ABRC)	SALK_130595
Arabidopsis: *ul4y*: *ul4y*	ABRC	SALK_029203
Arabidopsis: *ul18z*: *ul18z*	ABRC	SALK_089798
Arabidopsis: *arr1,10,12*: *arr1-3 arr10-5 arr12-1*	Argyros et al.[153]; ABRC	CS39992
Arabidopsis: *lst8-1-1*: *lst8-1-1*	ABRC	SALK_002459
Arabidopsis: *pARF3::N3xGFP*: *pARF3::N3xGFP*	Rademacher et al.[154]; ABRC	CS67072
Arabidopsis: *pARF6::N3xGFP*: *pARF6::N3xGFP*	Rademacher et al.[154]; ABRC	CS67078
Arabidopsis: *pARF8::N3xGFP*: *pARF8::N3xGFP*	Rademacher et al.[154]; ABRC	CS67082
Arabidopsis: *pARF10::N3xGFP*: *pARF10::N3xGFP*	Rademacher et al.[154]; ABRC	CS67086
Arabidopsis: GFP-nes: *pUBQ10::sfGFP-NES:UBQ3ter*	This study	N/A

(*Continued on next page*)

Continued

REAGENT or RESOURCE	SOURCE	IDENTIFIER
Arabidopsis: ARR7-llama GFP-nes: *pARR7::ARR7-llama pUBQ10:: sfGFP-NES:UBQ3ter*	This study	N/A
Oligonucleotides		
Primers	See Data S5	N/A
Recombinant DNA		
pARR7::ARR7:Llama	See Data S5	N/A
pUBQ10::sfGFP:NES:UBQ3ter	See Data S5	N/A

EXPERIMENTAL MODEL AND STUDY PARTICIPANT DETAILS

Plant material

Most Arabidopsis (*Arabidopsis thaliana*, RRID:NCBITaxon_3702) plants were in Col-0 background (WT). *ap1 cal 35S::AP1-GR* was in Ler background. *drmy1* (Col-0) was backcrossed to Ler twice and then crossed with *ap1 cal 35S::AP1-GR* to obtain *drmy1 ap1 cal 35S::AP1-GR*. The *ap1 cal AP1-GR* inflorescence produces numerous tightly packed ball-shaped meristems, which, upon induction, synchronously initiate sepal primordia, allowing us to collect large quantities of floral meristems with sepal primordia initiating (Stage 3)[34] (Figure S1A). R2D2 was originally in Col-Utrecht background and was backcrossed twice into WT (Col-0) and *drmy1* (Col-0). The following mutants and reporters were previously published: *drmy1-2*,[23] *wol-1*,[148] *spaghetti-1* (*tpr5-1*),[149] *ahp6*,[11] *arr3,4,5,6,7,8,9,15*,[94] *ap1 cal 35S::AP1-GR* (Ler),[32,33] *arr1-1 35S::ARR1*,[68] *DR5::3xVENUS-N7*,[150] *TCS::GFP*,[151] *pARF5::ER-EYFP-HDEL*,[152] *pUS7Y-mDII-NtdTomato-pUS7Y-DII-N3xVENUS* (R2D2),[102] *35S::mCirtine-RCI2A*,[23] *UBQ10::mCherry-RCI2A*,[23] *pAHP3::AHP3-GFP*,[93] *pAHP6::AHP6-VENUS*,[11] and *pAHP6::GFP-ER*.[11,90] The following mutants and reporter lines were obtained from Arabidopsis Biological Resource Center (ABRC): *ul4z* (SALK_130595), *ul4y* (SALK_029203), *ul18z* (SALK_089798), *arr1-3 arr10-5 arr12-1*[153] (CS39992), *lst8-1-1* (SALK_002459), *pARF3::N3xGFP*[154] (CS67072), *pARF6::N3xGFP*[154] (CS67078), *pARF8::N3xGFP*[154] (CS67082), *pARF10::N3xGFP*[154] (CS67086).

Llama-tagged ARR7 construct

For the LlamaTag system, we designed a construct with ARR7 fused with GFP-specific LlamaTag (*pARR7::ARR7-llama-ARR7ter*; *ARR7-llama* for short). This construct was co-transformed with cytoplasm-localized GFP containing a nuclear exclusion signal (*pUBQ10::sfGFP-nes-UBQ3ter*; *GFP-nes* for short; Figure 7C).

We first generated plasmid *pVV13* containing linker-llama. We amplified the LlamaTag (from a plasmid containing vhhGFP4[155]) and added a linker sequence of tccggagcagctgcggctgccgctgcggcagcggccactagt at its 5' end by two rounds of overlap PCRs. Primers for the first round were oVV64 and oVV53, and primers for the second round were oVV35 and oVV53. After the second round, we A-tailed the PCR product according to the Promega manufacturer's protocol. A-tailed product was ligated to the pGEMTeasy vector according to the Promega ligation protocol, to create the plasmid *pVV13*.

To make *pARR7::ARR7-llama*, a genomic fragment of *pARR7::ARR7* minus the stop codon and terminator was amplified from the Arabidopsis (Col-0) genome using the primers oSK197 and oSK198. The linker-llama fragment was PCR-amplified from *pVV13* using the primers oSK199 and oSK200. The *ARR7* stop codon, 3' UTR, and terminator was amplified from the Arabidopsis (Col-0) genome using the primers oSK201 and oSK202. *pMLBART* backbone was digested with NotI, and all fragments were assembled into *pMLBART* using NEBuilder according to the manufacturer's protocol.

To make *pUBQ10::sfGFP-NES:UBQ3ter*, sfGFP sequence was amplified from the *35S-sfGFP-nosT* plasmid[156] (Addgene # 80129) using primers UsfGM-F1 and UsfGnes-R1. The UBQ10 promoter was amplified from the *UPG* plasmid[157] (Addgene # 161003) using primers OutALFd and UsfGM-R1. The UBQ3 terminator was amplified from the *UPG* plasmid[157] (Addgene # 161003) using primers UsfGnes-F1 and OutALRb. Primer overhangs spanning the junction between sfGFP and the UBQ3 terminator contain the sequence of the mouse PKIα NES. *pCambia1300* backbone was digested with BamHI and KpnI, and all fragments were Gibson-assembled into the backbone. Sequences of primers, *pARR7::ARR7-llama*, and *pUBQ10::sfGFP-NES:UBQ3ter* can be found in Data S5.

Col-0 plants were co-transformed with *pARR7::ARR7-llama* and *pUBQ10::sfGFP-NES:UBQ3ter*, and selected with Basta (for *pARR7::ARR7-llama*) + Hygromycin (for *pUBQ10::sfGFP-NES:UBQ3ter*). Surviving T1 plants were screened for clear nuclear signal in the inflorescence, and 5 independent T1 plants were selected and crossed into *drmy1*. F2 plants from each line were again selected with Basta + Hygromycin and genotyped. One line showed co-segregation with the *DRMY1* locus. Two lines showed severe silencing in the F2 and could not be used. Two lines (7-4 and 7-6), though with minor silencing in F2, were used for imaging and image analysis. F3 plants of 7-4 and 7-6 had severe silencing, and therefore only F2 were imaged.

Plant growth conditions

For most experiments, seeds were sown in wetted Lamber Mix LM-111 soil and stratified at 4°C for 3-5 days. For experiments including *drmy1 wol* and *drmy1 arr1,10,12*, all seeds were sown onto ½ MS plates with 0.05% (w/v) MES, 1% (w/v) sucrose, 1.2% (w/v) agar, pH 5.7, and stratified at 4°C for a week. They were grown for 7-10 days before being transplanted to soil (for imaging of inflorescence or aerial part of the plant) or left on the plates until desired time of the experiment (for seedling imaging or puromycin labeling).

Most plants were grown under 16 h – 8 h light-dark cycles (fluorescent light, ~100 μmol m^{-1} s^{-1}) at 22°C in a Percival walk-in growth chamber. We found that the *drmy1* phenotype is more pronounced in this condition than under continuous light. The *ap1 cal 35S::AP1-GR* and *drmy1 ap1 cal 35S::AP1-GR* plants were grown in soil under continuous light at 16°C to prevent premature floral induction.

We note that we have used different tissue of different age in different experiments. 2-month-old induced inflorescences of *ap1 cal AP1-GR* background were used in transcriptomics (Figures 1B, S1B, S1C, S5A, S5B, and S7B), proteomics (Figures 1E, S1B, S1H, and S5A), polysome profiles (Figure 1C), and puromycin labeling (Figure 1D). Inflorescences that just bolted (6–10 weeks depending on the genotype) were used for confocal imaging. 8-day-old seedlings were used in TOR-inhibition transcriptomics (Figures 1F, 1G, S1I, and S1J) and TOR activity assay (Figures 1H and 1I) as these were established protocols in the lab. For puromycin labeling, 8-day-old WT seedlings and 10-day-old *drmy1* mutant seedlings were used in Figure 1D to match in size. 8- and 14-day-old seedlings were used in Figures 6A–6C as the cytokinin signaling mutant *wol* and *drmy1 wol* were extremely small and unable to match in size with WT and *drmy1* seedlings. These differences in plant tissue used were noted in the figure legends and also discussed below in the method details section.

METHOD DETAILS

Flower staging

Flower buds were staged as follows.[34] Stage 1 is when the floral meristem emerges, but not yet separated, from the inflorescence meristem. Stage 2 is when the floral meristem separates from the inflorescence meristem but with no floral organs initiated. Stage 3 is when sepal primordia initiate. Stage 4 is when sepal primordia bend to cover part of the floral meristem. Stage 5 is when stamen primordia initiate. Stage 6 is when sepal primordia completely cover the floral meristem.

RNA-seq data collection and analysis

For RNA-seq in the inflorescence, bolting *ap1 cal 35S::AP1-GR* and *drmy1 ap1 cal 35S::AP1-GR* plants were induced daily with an aqueous solution containing 10 μM dexamethasone (Sigma-Aldrich), 0.01% (v/v) ethanol, and 0.015% (v/v) Silwet L-77 (Rosecare.com). When sepals initiated from the floral meristems, usually on the fourth day after three daily inductions, three inflorescence samples per genotype (including inflorescence meristems and buds under stage 6) were collected and immediately ground in liquid nitrogen. RNA was extracted using RNeasy Plant Mini Kit (Qiagen, cat. no. 74904) following manufacturer's instructions. For library preparation, mRNA was isolated using Dynabeads (Invitrogen, cat. no. 61006) and fragmented in first strand buffer for 6 min at 94°C. First strand cDNA was synthesized with random hexamers (Invitrogen, cat. no. 48190011) and Superscript II (Invitrogen, cat. no. 18064014), and second strand DNA was synthesized with DNA Pol I (Fermentas, cat. no. EP0041) and RNase H (Invitrogen, cat. no. 18021071). End repair was performed using NEBNext End Repair Enzyme Mix (NEB, cat. no. E6050S) and Klenow DNA polymerase (NEB, cat. no. M0210S). A-tailing was performed using Klenow 3' to 5' exonuclease (Fermentas, cat. no. EP0421). DNA was ligated to NEBNext adaptors (NEB, cat. no. E7335L) using Mighty Mix Ligase (Clonetech, cat. no. TAK6023). Libraries were size selected using AMPure XP beads (Beckman Coulter, cat. no. A63880). PCR enrichment and barcoding was performed using NEBNext Multiplex Oligos for Illumina Index Primers (NEB, cat. no. E7335L) for 15 cycles using Phusion polymerase (NEB, cat. no. M0530L). Entire libraries were run on a 1.2% agarose gel in TAE buffer and size-selected in the 200-500 bp range. RNA-seq was performed in a NextSeq 500 machine (run length 75, single barcode) at Cornell Genomics Facility.

RNA-seq reads were quality-filtered using a custom Perl script (https://github.com/SchwarzEM/ems_perl/blob/master/illumina/quality_trim_fastq.pl) with parameters "-q 33 -u 84", and then trimmed using Trimmomatic (version 0.36)[158] with parameters "SE -phred33 [...] ILLUMINACLIP:[...]/sepal_ adapters_09dec2016.trimmomatic.fa:2:30:10 LEADING:3 TRAILING:3 SLIDINGWINDOW:4: 15 MINLEN:84". Trimmed reads were mapped to cDNA sequences of Arabidopsis (TAIR10) and quantified using Salmon (version 0.14.1).[159] Salmon arguments for indexing were "–no-version-check index -k 31 –perfectHash –type quasi –keepDuplicates". Salmon arguments for computing gene expression levels were "–no-version-check quant –seqBias –gcBias –validateMappings –libType A –geneMap TAIR10_cdna_20101214_updated_w_ GFP.tx2gene.tsv.txt –numBootstraps 200". Genes with at least two raw reads in at least two biological replicates in either WT or *drmy1* were kept for downstream analysis. DESeq2 (version 1.18.1)[160] was used to find differentially expressed genes, with a $\log_2$ fold change threshold of ±1 and a BH-adjusted p-value threshold of 0.05. For GO term enrichment, gene-GO mapping data was obtained from TAIR (https://www.arabidopsis.org /download_files/GO_and_PO_Annotations/Gene_Ontology_Annotations/ATH_GO_GOSLIM.txt). The R package "topGO"[161] (version 2.38.1) was used for the enrichment, with statistic "fisher", algorithm "weight01", annotation function "annFUN.gene2GO", and minimum node size 10. The results were ranked by their p-value, and the first 8 terms were plotted.

For RNA-seq in seedlings, WT and *drmy1* seedlings were grown to quiescence (7 days) in ½ MS liquid media.[31] After 7 days, the media was replaced with ½ MS liquid media containing 15 mM glucose and incubated for 24 hours to activate TOR. Seedlings were then incubated with or without AZD-8055 in addition to 15 mM glucose in ½ MS liquid media for 2 hours before collecting tissue. RNA was extracted from 100 mg pooled seedlings using the Spectrum Plant Total RNA Kit (Sigma). This RNA was used as a template for RNA-Seq library synthesis and sequencing, which was performed by Novogene. RNA-seq data for AZD-8055 treated WT and *drmy1* seedlings were preprocessed with fastp (version 0.22.0) using default parameters. Preprocessed reads were then mapped to the TAIR10 reference genome using STAR (version 2.7.10z_alpha_220314). Following alignment, BAM output files from STAR were used to generate feature counts for transcripts using subread-featureCounts (version 2.0.3) and the Araport11 transcriptome. TPMs were generated using TPMCalculator (version 0.0.3). Differential expression analysis was performed using feature count data and DESeq2 (version 1.36.0).

A list of genes with uORFs based on gene models of the TAIR10 Arabidopsis genome assembly were downloaded from von Arnim et al.[64] For each gene, within each genotype, protein-transcript ratio was calculated as the ratio between mean protein abundance and mean transcript TPM across all bio-reps in our proteomics and RNA-seq datasets, respectively. This was $\log_2$-transformed, and the difference between *drmy1* and WT was calculated. This was used as an indicator of translation rate difference between *drmy1* and WT, although we acknowledge that other factors such as protein stability may affect this number. This was plotted against the number of uORFs in each gene model (0, 1, or $\geq$ 2).

Proteomics

Five induced inflorescence samples of WT and *drmy1* in *ap1 cal AP1-GR* background were collected as described above. Samples were ground in liquid nitrogen. Total soluble proteins were extracted in ice-cold extraction buffer (50 mM PBS-HCl (pH 8.0) buffer with 150 mM NaCl, 2% NP-40, 1 mM PMSF, 1x Roche cOmplete protease inhibitor cocktail (Sigma 11697498001), and 1x Halt TM Phosphatase inhibitor cocktail (ThermoFisher 78420)) and filtered through Pierce™ Micro-Spin Columns (30 μm pore size; Thermo Scientific 89879). Extracts were RuBisCO-depleted using Seppro Bubisco Kit (Sigma SEP070-1KT), concentrated, denatured, reduced, cysteine blocked, trypsin-digested, and TMT 10-plex labeled. Then, mass spectrometry was done using an UltiMate 3000 RSLCnano / Orbitrap Fusion system (Thermo Scientific). Raw data was searched against the NCBI protein database using PD 2.3 (Thermo Scientific) with Sequest HT searching engine. Precursor-based protein identification and relative quantification was done using the standard processing workflow in PD 2.3, with an additional node of Minora Feature Detector. Proteins with at least 2 supporting peptides were kept for downstream analysis. For each protein, data was fit with an ANOVA model and a p-value was calculated. Proteins with a p-value < 0.05 were considered differentially accumulated in *drmy1*. GO term enrichment was done as above, using genes corresponding to the differentially accumulated proteins.

Polysome extraction and profiling

Three induced inflorescence samples of WT and *drmy1* in *ap1 cal AP1-GR* background were collected as described above. For polysome extraction,[162] samples were ground in liquid nitrogen, mixed with an extraction buffer twice the volume of pulverized tissue (0.2 M Tris pH 9.0, 0.2 M KCl, 0.025 M EGTA, 0.035 M $MgCl_2$, 1% (w/v) Brij-35, 1% (v/v) Triton X-100, 1% (v/v) Igepal CA-630, 1% (v/v) Tween-20, 1% (w/v) Sodium deoxycholate, 1% (v/v) Polyoxyethylene 10 tridecyl ether, 5 mM Dithiothreitol, 1 mM Phenylmethylsulfonyl fluoride, 100 μg/ml cycloheximide, 100 μg/ml chloramphenicol, 40 U/ml RNasin, 10 U/ml DNase I), and let sit on ice for 10 min. Samples were centrifuged at 4°C 4,000 g for 5 min, supernatant was transferred to a new tube, centrifuged at 4°C 16,000 g for 15 min, and supernatant was filtered through Miracloth.

For profiling of polysome extracts,[163] 600 μl of each sample were loaded onto a 15%–45% sucrose density gradient and centrifuged at 4°C 32,000 rpm in a SW41 rotor. Separated samples were fractionated at a rate of 0.375 mL/min in an Isco fractionation system, and absorbance at 254 nm was recorded.

Puromycin labeling

In seedlings, when comparing WT and *drmy1*, in order to control for plant size, WT seedlings were grown for 8 days and *drmy1* seedlings were grown for 10 days (Figure 1E). When comparing WT, *drmy1*, *wol*, and *drmy1 wol*, we were unable to control for plant size because *wol* and *drmy1 wol* seedlings were too small. We therefore controlled for plant age, and seedlings were grown to specified age (8 days for Figure 6B and 14 days for Figure 6C). Seedlings were harvested from plates and incubated with an incubation buffer (½ MS, 0.05% (w/v) MES, 1% (w/v) sucrose, 0.1% (v/v) Tween-20, 0.1% (v/v) DMSO, 1x Gamborg vitamin mix, pH 5.7), with or without 50 μM CHX, for 4 hours in an illuminated growth chamber. Then, the buffer was replaced with a fresh incubation buffer (which is same as above, but contains 50 μM puromycin (GoldBio P-600-100)), and incubation continued for another 45 min.

In inflorescences of WT and *drmy1* in *ap1 cal AP1-GR* background, inflorescences were DEX-induced as described above. Inflorescence samples were collected and put in an incubation buffer (½ MS, 1% (w/v) sucrose, 0.02% (v/v) Silwet L-77, 0.1% (v/v) DMSO, 50 μM puromycin, 1x Gamborg vitamin mix, pH 5.7), with or without 100 μM CHX. Samples were vacuum infiltrated for 15 minutes and then put on a rocking shaker in an illuminated growth chamber for 45 minutes.

In both cases, at the end of the incubation, samples were washed three times with water, blot dry, weighed, and frozen in liquid nitrogen. Soluble proteins were extracted as described above. Puromycin incorporated into the proteins were detected in a Western blot using a mouse-origin anti-puromycin monoclonal antibody (12D10, Sigma MABE343, lot # 3484967) and a goat-anti-mouse HRP-conjugated secondary antibody (Abcam ab6789, lot # 3436981). RuBisCO large subunit in Ponceau S-stained membrane was used as a loading control. Quantification was done in ImageJ. A background signal was determined using blank regions, and subtracted from all quantified signals (separately for puromycin and Ponceau S).

TOR activity assay

WT and *drmy1* seedlings were grown in a six-well plate containing ½ MS liquid media. After 7 days, the media were replaced with half-strength MS liquid media plus 15 mM glucose and incubated for 24 hours. At least 120 quiescent seedlings per sample were collected and frozen in liquid nitrogen. Protein was then extracted from the plant tissue in 100 mM MOPS (pH 7.6), 100 mM NaCl, 5% SDS, 0.5% b-mercaptoethanol, 10% glycerin, 2 mM PMSF, and 1x PhosSTOP phosphatase inhibitor (Sigma). S6K-pT449 was detected by Western blot using a phosphospecific antibody (Abcam ab207399) and an HRP-conjugated goat anti-rabbit IgG secondary antibody (Jackson Immuno Research 111-035-003). Total S6K was detected using a custom monoclonal antibody.[164] Total protein visualized in Ponceau S-stained membrane was used as a loading control.

Confocal microscopy

Main inflorescences (not side branches) were cut and dissected with a Dumont tweezer (Electron Microscopy Sciences, style 5, no. 72701-D) to remove buds older than stage 9 or 10. The inflorescences were then inserted upright into a small petri dish (VWR, 60 x 15 mm) containing inflorescence culture medium (1/2 MS, 1% (w/v) sucrose, 1x Gamborg vitamin mixture, 0.1% (v/v) plant preservative mixture (Plant Cell Technology) 1% (w/v) agarose, pH 5.8), leaving most of the stem inside the medium and the buds outside. They were then further dissected to reveal stage 6 and younger buds, immersed with water, and imaged under a Zeiss710 upright confocal microscope with a 20x Plan-Apochromat water-dipping lens (1.0 NA). For live imaging experiments, inflorescence samples were put in a continuous-light growth chamber between time points. To prevent bacterial growth, samples were transferred onto fresh media every 2 to 3 days, and for live imaging experiments lasting longer than 6 days, once in the middle, plants were incubated with an aqueous solution of 100 μg/ml Carbenicillin (GoldBio, C-103-5, lot # 0129.091814A) for 30 minutes.

To visualize tissue morphology of inflorescence samples without a reporter, samples were stained for 5 minutes with an aqueous solution of 0.1 mg/ml propidium iodide (PI) and 0.1% (v/v) Tween-20, washed three times with water, and imaged.

The following laser and wavelength were used in confocal imaging. Chlorophyll, excitation 488 nm, emission 647-721 nm. PI, excitation 514 nm, emission 566-659 nm. mCherry, excitation 594 nm, emission 600-659 nm. tdTomato, excitation 561 nm, emission 566-595 nm. For EYFP/VENUS/mCitrine, in *35S::mCirtine-RCI2A*, excitation 514 nm, emission 519-580 nm; in *DR5::3xVENUS-N7*, excitation 514 nm, emission 519-569 nm; in *pARF5::ER-EYFP-HDEL*, excitation 514 nm, emission 519-550 nm; in *R2D2*, excitation 488 nm, emission 493-551 nm. For GFP/sfGFP, in *pARR7::ARR7-llama UBQ10::sfGFP-NES*, excitation 488 nm, emission 493-569 nm; in *pARF3::N3xGFP*, *pARF6*::N3xGFP, *pARF8::N3xGFP*, and *pARF10::N3xGFP*, excitation 488 nm, emission 493-564 nm; in *TCS::GFP*, excitation 488 nm, emission 493-513 nm.

Visualization of tissue morphology

For single-channel image stacks intended for the visualization of tissue morphology (*35S::mCitrine-RCI2A* or PI), stacks were 3D-rendered using the ZEN confocal software (Processing -> 3D). Parameters were set to best visualize tissue morphology, typically, minimum 5-10, ramp 60-80, maximum 100. Buds were rotated to desired orientation, and screenshots were taken using the "Create Image" button. For fluorophores that are dimmer, less sharp, or have a noisy background (*UBQ10::mCherry-RCI2A* or Chlorophyll), stacks were converted from LSM to TIF using ImageJ,[165,166] loaded into MorphoGraphX,[167] and screenshots were taken using the built-in screenshot function in MorphoGraphX.

To aid visualizing tissue morphology and determine the timing of sepal initiation, each stack was fitted with a surface, and a Gaussian curvature heatmap was calculated from the surface (see below). We consider a sepal primordium as initiated when we see a dark red band of positive Gaussian curvature (primordium) separated from the center of the floral meristem by a dark blue band of negative Gaussian curvature (boundary).[23]

To generate Gaussian curvature heatmaps, stacks underwent the following processes in MorphoGraphX: Gaussian blur (3 times; X/Y/Z sigma = 1 μm for the first 2 times, and 2 μm for the third time), edge detection (threshold = 2000-8000 depending on the brightness of the stack, multiplier = 2.0, adapt factor = 0.3, fill value = 30000), marching cube surface (cube size = 8 μm, threshold = 20000), subdivide mesh, smooth mesh (passes = 5), subdivide mesh, smooth mesh (passes = 5), project mesh curvature (type = Gaussian, neighborhood = 10 μm, autoscale = no, min curv = -0.0015, max curv = 0.0015). For ease of visualization, the lookup table "jet" was applied to the mesh.

Quantification of sepal initiation robustness

For sepal primordium number, screenshots were taken of stage 3-6 buds of indicated genotypes, in either ZEN or MorphoGraphX. The number of sepal primordia initiated were counted from these screenshots.

For variability in sepal primordium positioning, within each bud, an angular distance was measured between each pair of adjacent sepal primordia (with vertex at the center of the bud), using ImageJ. Note that the last pair was not measured – the angular distance was calculated as the sum of all other angular distances subtracted from 360°. A CV value (standard deviation divided by mean) was calculated from all the measured or calculated angular distances. Buds with sepal primordia evenly distributed around the bud periphery should have a small CV value, i.e. all angles are around 90° for four-sepal buds (or 72° for five-sepal buds, etc.). Buds whose sepal primordia distributed variably or randomly around the bud periphery will have widely varying angular distances between adjacent sepal primordia, and thus large CV values.

To quantify relative sepal initiation timing, dissected inflorescence samples were live-imaged every 6 hours. A Gaussian curvature heatmap was generated for each sample at each time point and was used to determine the time point at which a sepal primordium initiates. A sepal primordium is considered initiated at time point Tn if it is absent at time point T(n-1) but becomes present at time point Tn. Within the same bud, we counted the number of time points between outer and inner sepal initiation, and between outer and lateral sepal initiation, and multiplied them by 6 hours to get the relative initiation timing of these sepals.

Quantification of fluorescent reporters

For *TCS::GFP*, *pARF3::N3xGFP*, *pARF5::ER-YFP-HDEL*, *pARF6::N3xGFP*, *pARF8::N3xGFP*, *pARF10::N3xGFP*, *pUS7Y::mDII-NtdTomato, pUS7Y::DII-N3xVENUS*, and *UBQ10::mCherry-RCI2A*, total signal (integrated density) was quantified from maximum intensity projection images using ImageJ.[165,166] Fluorescence intensity was measured in pixel intensity units (0-255 range). Signal intensity was calculated as total signal divided by area.

For both *TCS::GFP* and *DR5:3xVENUS-N7*, circular histogram analysis was performed as follows. Individual buds were cropped out of image stacks, channels were split using ImageJ and saved in TIF format, and TIF stacks were imported into MorphoGraphX. Signal from outside the buds (e.g. inflorescence meristem, parts of other buds within the same image) was manually removed using the Voxel Edit function. Buds were positioned so that the incipient sepal primordia are in the XY plane: the incipient outer sepal is at 45°, the incipient inner sepal and the inflorescence meristem are at 225°, and the incipient lateral sepals are at 135° and 315°, respectively. Each bud was divided into 360 sectors of 1° each; within each sector, signal measured in pixel intensity units (0-255 range) was summed. A circular histogram was generated starting at 0° (between the incipient outer and right sepals) going counterclockwise. Multiple circular histograms of the same reporter and genotype were pooled; mean was plotted as a solid line, and mean±SD was plotted as a shaded area.

For GFP signal in plants carrying *pUBQ10::sfGFP-nes-UBQ3ter* and *pARR7::ARR7-linker-llama-ARR7ter* reporters, screenshots were taken in MorphoGraphX as described above. Screenshots were subtracted of a background determined using blank regions with no tissue, and brightened to the same level to reveal differences in GFP distribution patterns. A square region containing 5-10 cells were taken from each screenshot, and GFP intensity (in gray value ranging from 0 to 255) along a straight line of 239 pixels in length was quantified using ImageJ[165,166] (Analyze -> Plot profile). For ease of visualization, the curves were smoothed by taking the average of the gray value of 11 neighboring pixels (including itself) as the value of each pixel.

For VENUS or GFP signal in *pAHP6::AHP6-VENUS*, *pAHP6::GFP-ER*, *pAHP3::AHP3-GFP*, and *pUBQ10::mCherry-RCI2A* under mock, CHX, or AZD-8055 treatment, total signal at 24 hours (for CHX) or 72 hours (AZD-8055) was normalized by bud area in the 2D projection to get the signal intensity. To account for bud-to-bud differences in signal intensity prior to treatment, the signal intensity was normalized to the 0-hour time point (pre-treatment). Relative level between treatment and mock was calculated by normalizing this value to the mean of mock.

In vitro drug treatments on inflorescence samples

For cycloheximide (CHX) treatment, a stock solution of 10 mM CHX was made from powder (Sigma C1988) in pH 4.0 water. The stock was filter-sterilized and stored in -20°C, and added to autoclaved inflorescence culture medium to a final concentration of 2 μM just before use. For AZD-8055 treatment, a stock solution of 16 mM AZD-8055 was prepared from powder (Cayman Chemical 16978) in DMSO within days of use, and stored in -80°C. The stock was added to autoclaved inflorescence culture medium to a final concentration of 2 μM. 0.0125% (v/v) DMSO was added to the mock medium. For 6-benzylaminopurine (BAP) treatment, a stock solution of 50 mM BAP was prepared from powder (Alfa Aesar A14678) in DMSO, and stored in -80°C. The stock was added to autoclaved inflorescence culture medium to a final concentration of 5 μM. 0.01% (v/v) DMSO was added to the mock medium.

Inflorescences were dissected and inserted into regular inflorescence culture medium without drugs, and pre-treatment image stacks were captured. Then, they were transferred into specified treatment or mock media, and imaged at the specified time points. For live imaging, inflorescence samples were transferred onto new medium after each imaging session.

Torin2 and AZD-8055 treatment in planta

Starting at 14 days after germination, twice each day for 15 days, 20 μl of 100 μM Torin2 (Cayman Chemical 14185) or 3.2 μM AZD-8055 (Cayman Chemical 16978) containing 0.5% DMSO and 0.5% Tween-20 was applied to the center of the rosette using a pipette. For mock, 20 μl water containing 0.5% DMSO and 0.5% Tween-20 was applied. At the end of the 15-day treatment period, inflorescences were dissected and put in the inflorescence culture medium for imaging. To prevent drug degradation, throughout the duration of this experiment, the AZD-8055 and Torin2 stock solutions was kept in -80°C and replaced each week, and the treatment and mock solutions were kept in 4°C and replaced each day.

Imaging of whole plant, whole inflorescence, silique, and mature sepals

For whole-plant imaging, aerial parts of the plants were removed from the pots, flattened, put on a dark cloth, and imaged with a cell phone (iPhone 12, iOS 16.2).

For whole-inflorescence imaging, inflorescences consisting of open flowers and unopened buds were removed from the plant and held with forceps. Images were taken under a Zeiss Stemi 2000-C Stereo Microscope with a cell phone (iPhone 12, iOS 16.2).

For silique imaging, siliques on inflorescences sufficiently distant from the shoot apex that were developed and started to ripen were picked with forceps, opened with a razor blade, and imaged under a Zeiss Stemi 2000-C Stereo Microscope with a cell phone (iPhone 12, iOS 16.2).

For mature sepal imaging, mature sepals from stage 15 flowers (10^{th} to 25^{th} flower on the inflorescence) were dissected and sandwiched between two slides to flatten. Images were taken using a Canon Powershot A640 camera attached to a Zeiss Stemi 2000-C Stereo Microscope. Minor damages were manually fixed, and undesired objects such as pollen grains were manually removed from these images. Sepals with major damages were discarded. Then, a contour was extracted from each sepal using custom python scripts.[21] This gave us measurements such as length, width, area, etc. of each sepal. To measure between-flower variability of length, within each genotype and for each of outer, inner, and lateral positions, a CV (standard deviation divided by mean) of all sepals was calculated (for example, a CV of length of all outer sepals in WT). To determine statistical significance, genotypes were compared pairwise using permutation tests. To measure within-flower variability of length, a CV was calculated for all sepals within each flower (for example, a CV of length of outer, inner, and two lateral sepals in WT bud #10). For accurate calculation of CV, flowers with length data of at least four sepals were included in the analysis. To determine statistical significance, genotypes were compared pairwise using Wilcoxon rank sum tests.

Cytokinin extraction and measurement

For cytokinin extraction,[168] five inflorescence samples of induced *ap1 cal 35S::AP1-GR*, and six inflorescence samples of induced *drmy1 ap1 cal 35S::AP1-GR* were collected as described above. Samples were ground in liquid nitrogen and twice extracted in methanol: water: formic acid (15:4:1). 200 pg of BAP per sample was added as an internal control. Extracts were centrifuged at 14,650 rpm in -4°C for 30 min, and supernatant was evaporated of methanol and reconstituted in 1% (v/v) acetic acid. Samples were passed through an Oasis MCX SPE column (Waters 186000252), washed with 1% acetic acid, washed with methanol, and eluted with 0.35 M ammonia in 70% methanol. Eluents were evaporated to complete dryness, reconstituted in 5% acetonitrile, and sent for LC-MS.

For LC-MS,[169] 1 μl of each sample was injected into a Thermo Fisher Scientific Vanquish Horizon UHPLC System coupled with a Thermo Q Exactive HF hybrid quadropole-orbitrap high-resolution mass spectrometer equipped with a HESI ion source. Samples were separated on a C18 ODS column (AQUITY UPLC BEH C18, 1.7 μm, 2.1 × 100 mm, Waters), at a flow rate of 0.3 ml/min, with linear gradients of solvent A (0.1% formic acid) and solvent B (0.1% formic acid in methanol) according to the following profile: 0 min, 99.0% A + 1.0% B; 4.0 min, 55.0% A + 45.0% B; 7 min, 30.0% A + 70.0% B; and then with isocratic conditions: 8 min, 1.0% A + 99.0% B; 12 min, 99.0% A + 1.0% B. Cytokinins were detected using the positive ion mode.

For tZ, tZR, iP, iPR, and the internal control BAP, peaks were identified from an external standard mix composed of 0.1 μg/ml each of BAP (Alfa Aesar A14678), tZ (Sigma Z0876), tZR (Sigma Z3541), iP (Cayman Chemical 17906), and iPR (Cayman chemical 20522) in 5% acetonitrile. For cZ and cZR, peaks were identified based on previously reported precursor m/z and retention time.[170] Using Xcalibur (Thermo Scientific), peak area was quantified for each cytokinin in each sample, normalized against the peak area of BAP (internal control) and sample fresh weight, and then normalized against the average abundance of tZ in WT samples.

Image processing software

Image processing was done in ImageJ (version 2.9.0/1.53t, build a33148d777)[165,166] and MorphoGraphX (version 2.0, revision 1-294, CUDA version 11.40).[167] Figures were assembled in Adobe Illustrator (version 25.4.1). An RGB color profile "Image P3" was used for all the figures.

QUANTIFICATION AND STATISTICAL ANALYSIS

Statistical tests

Pairwise numerical differences in mean were determined using Student's two-sided t-tests (Figures 1D, 1I, 4B, 4F, 4J, 6A–6C, S4G, and S4K), Wilcoxon's rank sum tests (Figures 2J, 2R, 3C, 3F, 5G, 5N, 7Q, S2J, S3N, S5A, S5D, S7A, and S7P), or permutation tests (Figure S3M). Pairwise numerical differences in variation were determined using Levene's tests (Figures 3C and 3F). Categorial differences were determined using Fisher's contingency table test (Figures 2H, 2Q, 5F, 5M, 7P, and S2I) or Chi-square test (Figure S1I). Two factor data were fit using ANOVA (Figure S1G). Gene ontology enrichment was determined using Fisher's exact test (Figures 1B, 1E, and S1J). Correlation was assessed using linear regression (Figure 1F). Statistical details can be found in the figures, figure legends, and main text.

Statistical software

Data processing was done in RStudio (R version 4.0.5 "Shake and Throw" (2021-03-31)).[171] Graphs were made using the package ggplot2 (version 3.3.3).[172] Differential gene expression in RNA-seq was determined in DESeq2.[160] Gene ontology enrichment tests were done using the topGO package[161] (version 2.38.1). Fisher's contingency table tests were done using the function fisher.test in R. Wilcoxon rank sum tests were done using the function wilcox.test in R. Levene's tests were done using the function leveneTest in the car package in R. Hypergeometric tests were done using the function phyper in R. Data fitting with ANOVA was done using the function aov in R.